New exact multi-coated ellipsoidal inclusion model for anisotropic thermal conductivity of composite materials

Napo Bonfoh, Florence Dinzart, Hafid Sabar

New exact multi-coated ellipsoidal inclusion model for anisotropic thermal conductivity of composite materials

Napo Bonfoh*, Florence Dinzart, Hafid Sabar

Laboratoire d'Etude des Microstructures et de Mécanique des Matériaux (LEM3), UMR CNRS 7239 - Université de Lorraine, CNRS, Arts et Métiers Paris Tech, LEM3, F-57000 Metz, France

Abstract

The present study deals with a new micromechanical modeling of the thermal conductivity of multi-coated inclusion-reinforced composites. The proposed approach has been developed in the general frame of anisotropic thermal behavior per phase and arbitrary ellipsoidal inclusions. Based on the Green's function technique, a new formulation of the problem of multi-coated inclusion is proposed. This formulation consists in constructing a system of integral equations, each associated to the thermal conductivity of each coating and the reference medium. Thanks to the concept of interior- and exterior-point Eshelby's conduction tensors, the exact solution of the problem of multicoated inclusion is obtained. Analytical expressions of the intensity in each phase and the effective thermal conductivity of the composite, through homogenizations schemes such as Generalized self-consistent and Mori-Tanaka models are provided. Results of the present model are successfully compared with those issued from both analytical models and finite elements methods for composites with doubly coated inclusions. Moreover, the developed micromechanical model has been applied to a three phase composite materials in order to analyze combined effects of the aspect ratio and the volume fraction of the ellipsoidal inclusions, the anisotropy of the thermal conductivity of interphase, the thermal conductivity contrast between local phases on the predicted effective thermal conductivity.

* Corresponding author.
E-mail address: napo.bonfoh@univ-lorraine.fr (N. Bonfoh)

Keywords: Composite materials; Anisotropic thermal conductivity; Multi-coated ellipsoidal inclusion; Generalized Self-Consistent scheme, Generalized Mori Tanaka model.

1. Introduction

In the last decades, composite materials have been undergoing continual technological evolutions and developments which have spread their use to many industry sectors. These composite materials are designed through a smart combination of inclusions embedded in a matrix in order to enhance some specific properties. Thermal conductivity appears as key property for many industrial applications such as electronics, thermal insulation, automotive and aeronautics. Recent developments of electronics devices have led to the optimization of heat dissipation. For this purpose, some composite materials may be tailored as a combination of highly conducting inclusions embedded in soft matrix to favor their manufacturing. During these processes, a thin interphase layer can appear between matrix and inclusions resulting from sizing, chemical reactions or low wettability. Furthermore, to improve the interfacial bonding between inclusions and matrix, a third constituent may be introduced between inclusions and matrix [1–3]. This interphase layer significantly affects local thermal fields and has to be taken into account for a rigorous prediction of effective properties that reveals to be a key step in the design and the manufacture of composite materials. Numerous theoretical studies have been devoted to the prediction of these effective properties, based on topological and morphological textures of the composite material. Homogenization methods based on multi-scale transitions methods provide a valuable tool for the design of new composite materials; they also allow to characterize the interphase through an inverse method. For particles reinforced composite materials, reported homogenization approaches are mainly based on Eshelby's inclusion model [4]. The topology of this model assumes that an ellipsoidal inclusion subjected to a uniform eigenstrain is embedded in a uniform infinite matrix. The solution of such a heterogeneous problem as provided by Eshelby's model established that strain field inside the ellipsoidal inclusion is uniform when the infinite matrix undergoes to uniform

remote strain. This pioneering Eshelby's model has been successfully applied for some homogenization schemes for heterogeneous materials (Dilute medium, Mori-Tanaka, Self-consistent, etc.) However, results issued from Eshelby's model are not relevant for moderate or high-volume fractions of inclusions, for rigids inclusions or voids [5], and also for heterogeneous materials with interphase.

In order to address these shortcomings, Eshelby's model has been extended to the case of coated inclusion in a matrix. Thus, the obtained model of coated inclusion gave rise to some more relevant homogenization schemes, able to deal with materials with complex microstructure. Among these, is generalized self-consistent (GSC) scheme that derived from the solution of the coated inclusion problem appears as a sophisticated homogenization method, combining both mathematical rigor and physical realism. In elasticity, GSC model promoted by Christensen [6], Christensen and Lo [7] provides satisfactory results, in agreement with experimental data, even for high volume fractions of inclusions, for voids or rigid inclusions.

However, the problem of coated inclusion in a general framework of arbitrary morphology and anisotropic behavior of the phases is a very complicated micromechanical problem. In addition, due to the complex interactions between the inclusion, the interphase and the matrix, local intensity fields are not uniform. Nevertheless, many studies have been devoted to the problem of coated inclusion in order to capture the effect of interphase on the effective thermal conductivity of composite materials. Depending on the considered approach, these investigations can be gathered into two categories:

- The first class originates from well-known works of Maxwell [8] and Rayleigh [9] that proposed the solution of Laplace's equation in terms of spherical harmonic function, for a two-phase material with isotropic thermal conductivity. From this fundamental result, Hashin and Shtrikman [10] derived the famous lower and upper bounds of the thermal conductivity in a macroscopically isotropic two-phase material. In this context, Hashin [11] determined the thermal

conductivity of an isotropic two-phase material in the framework of the generalized self-consistent (GSC) scheme. In isotropic conductivity, Herve [12] also obtained the effective thermal conductivity of multiply coated spherical inclusion-reinforced composites in the so-called '(N+1)-phase' GSC scheme. Yang [13] extended this approach to cylindrical inclusions. In the case of arbitrary ellipsoidal inclusions, the solution of Laplace's equation is obtained thanks to ellipsoidal harmonic functions and potential theory developed by Kellogg [14]. Based on this approach due to Kellogg [14], Stepin [15] obtained the solution of the problem of coated ellipsoidal inclusion imbedded in an infinite matrix, for isotropic thermal conductivity. Hatta and Taya [16], by using spheroidal harmonic functions, expressed the effective thermal conductivity for coated spheroidal inclusions by solving the fundamental Laplace's equation governing heat transfer. Then, Giordano [17] extended the solution due to Stepin [15] to an inclusion with anisotropic thermal conductivity. Benveniste et *al.* [18] proposed a model to predict the effective thermal conductivity of composite materials containing long fibers with transverse isotropic thermal conductivity.

Recently, Kolesnikov et *al*. [18], Lavrov and Yakovlev [19] extended the solution of coated inclusion problem as proposed by Giordano [17] and Stepin [15], to the case of anisotropic thermal conductivity. All above-mentioned models assume a uniform intensity field inside inclusion. The obtained solutions for an arbitrary morphology of ellipsoid inclusion (sphere, cylinder and ellipsoid) are analytical and compact. In the cases of spherical or cylindrical inclusion and isotropic thermal conductivity per phase, these expressions are exact since the intensity field remains uniform inside the inclusion. In contrast, for ellipsoidal inclusion and an anisotropic thermal conductivity per phase, the intensity field inside the inclusion is strongly disturbed by the presence of the coating and therefore this basic assumption appears uncertain.

- The second class of models deals with the Green's function technique and integral equation for the problem of heterogeneous thermal conductivity. For the coated inclusion problem, the integral equation exhibits a volume integral due to the presence of interphase. This volume integral

is difficult to compute, since both Eshelby's tensors and intensity fields are not uniform inside the interphase. Hori and Nemat-Nasser [21] proposed analytical expressions of local fields and effective properties of heterogeneous materials with the multi-coated inclusion. For an easy evaluation of the above-mentioned volume integral, this model assumes uniform elastic fields in the interphase. Then, the model was adapted to the prediction of effective thermal conductivity [22-24]. However, the model of Hori and Nemat-Nasser [21] is not exact and does not recover the solution of particular spherical and cylindrical morphologies of inclusions. Aboutajeddine and Neale [25] suggested an improvement of Hori and Nemat-Nasser's model [21] by confining interactions between the phases to direct interaction between the inclusion and its immediate environment. This assumption led to the cancellation of the integral term due to the presence of the interphase. This improved model was then extended to the problem of multi-coated inclusion in elasticity by Dinzart et *al*. [26] and in thermal conductivity by Dinzart et *al*. [27].

Up to now, the exact solution of coated ellipsoidal inclusions and anisotropic thermal conductivity per phase is not reported in the literature and therefore remains a challenge.

The present study therefore proposes a new micromechanical approach to deal with multi-coated ellipsoidal inclusion and anisotropic thermal conductivity per phase. The considered method is based on the Green's function technique and the integral equation of the problem of thermal conduction in heterogeneous mediums. New integral equations are formulated by introducing a Green's tensor for each anisotropic coating, in addition to the classical Green's tensor associated to the reference medium. The resolution of the corresponding system of integral equations is completed thanks to the concept of interior- and exterior-point Eshelby's conduction tensors. Moreover, the obtained solution provides exact analytical expressions of intensity inside inclusion and each coating, for composite material with multi-coated confocal ellipsoidal inclusions. The present model is applied for simply-coated and doubly-coated and obtained expressions are compared with those available in the literature. Then, GSC scheme and Generalized Mori-Tanaka

model are implemented to predict the effective thermal conductivity of composite materials containing multi-coated inclusions. The ability of the model to describe the thermal behavior of composite materials, for moderate or high-volume fractions of inclusions is discussed through some comparisons with numerical results issued from finite elements methods. Finally, some parametric analyses of the effects of the morphology and volume fraction of inclusions, the thickness of coatings and the contrast between local thermal conductivities on the predictions of the model are conducted and discussed.

2. Micromechanical model

2.1. Local constitutive laws and integral equation

The considered representative volume element (RVE) of the composite is a heterogeneous medium with linear thermal behavior described by the tensor $\boldsymbol{k}(\boldsymbol{r})$ at an arbitrary point $\boldsymbol{r}$ of Cartesian coordinates (x_1, x_2, x_3). The composite material is made of ellipsoidal inclusions surrounded by coatings, embedded in a matrix material. The inclusion, coatings and matrix are homogeneous and have a linear thermal behavior. The RVE is subjected to a uniform intensity $\boldsymbol{e}^0$ at its boundary. The interfaces between the constituents of the composite are assumed perfect. The present section aims at determining the temperature $T(\boldsymbol{r})$, intensity $\boldsymbol{e}(\boldsymbol{r})$ and heat flux $\boldsymbol{q}(\boldsymbol{r})$ fields in each phase and the effective thermal conductivity of the composite material. The fields equations of such a heterogeneous thermal conductivity problem are:

- intensity field related to the temperature field:

$$\boldsymbol{e}(\boldsymbol{r}) = -\boldsymbol{\nabla} T(\boldsymbol{r}) \tag{1}$$

- linear thermal behavior described by Fourier's law:

$$\boldsymbol{q}(\boldsymbol{r}) = \boldsymbol{k}(\boldsymbol{r}).\boldsymbol{e}(\boldsymbol{r}) \tag{2}$$

- energy conservation equation in steady state without thermal energy generation:

$$div\boldsymbol{q}(\boldsymbol{r}) = 0 \tag{3}$$

- boundary conditions

$$T^0(\boldsymbol{r}) = -\boldsymbol{e}^0.\boldsymbol{r} \quad \text{on} \quad \partial V \tag{4}$$

The notation $\boldsymbol{\nabla}$ stands for the gradient and the symbol '.' for the product of tensors and/or vectors. The local thermal conductivity $\boldsymbol{k}(\boldsymbol{r})$ is then split into a uniform part $\boldsymbol{k}^0$ of a Homogeneous Reference Medium (HRM) and a fluctuating one $(\boldsymbol{r})$:

$$\boldsymbol{k}(\boldsymbol{r}) = \boldsymbol{k}^0 + \delta\boldsymbol{k}(\boldsymbol{r}). \tag{5}$$

Thanks to Eq.(5), the local thermal behavior Eq.(2) becomes :

$$\boldsymbol{q}(\boldsymbol{r}) = \boldsymbol{k^0}.\boldsymbol{e}(\boldsymbol{r}) + \delta\boldsymbol{k}(\boldsymbol{r}).\boldsymbol{e}(\boldsymbol{r}). \tag{6}$$

In the present study, within the framework of thermal conductivity we develop the concept of projection operators initially promoted in elasticity by Kunin [24]. The projection operator $\boldsymbol{\Pi}^0$ associated to the HRM with thermal conductivity $\boldsymbol{k}^0$ is defined by:

$$\boldsymbol{\Pi}^0 = \boldsymbol{\Gamma}^0.\boldsymbol{k}^0 \tag{7}$$

$\boldsymbol{\Gamma}^0$ is the modified Green's conduction tensor defined by:

$$\boldsymbol{\Gamma}^0 = -\boldsymbol{\nabla}\boldsymbol{\nabla}G^0. \tag{8}$$

The Green's conduction function G^0 associated to HRM results from:

$$k_{ij}^0 \frac{\partial^2 G^0(\boldsymbol{r}-\boldsymbol{r}')}{\partial x_i\, \partial x_j} + \delta(\boldsymbol{r}-\boldsymbol{r}') = 0 \quad \text{and} \quad \lim_{|\boldsymbol{r}-\boldsymbol{r}'|\to\infty} G^0(\boldsymbol{r}-\boldsymbol{r}') = 0 \tag{9}$$

$\delta(\boldsymbol{r}-\boldsymbol{r}')$ is the Dirac delta function. The projection operator $\boldsymbol{\Pi}^0$ exhibits some properties that allow to rewrite Eqs. (1) and (3) as (see Appendix A):

$$\boldsymbol{e} = -\boldsymbol{\nabla}T \text{ and } T = -\boldsymbol{e}^0.\boldsymbol{r} \quad \text{on} \quad \partial V \Leftrightarrow \boldsymbol{\Pi}^0 * \boldsymbol{e} = \boldsymbol{e} - \boldsymbol{e}^0; \tag{10}$$

$$div\boldsymbol{q} = 0 \Leftrightarrow \boldsymbol{\Pi^0} * \boldsymbol{h}^0.\boldsymbol{q} = 0 \quad \text{with} \quad \boldsymbol{h}^0 = \boldsymbol{k}^{0^{-1}}. \tag{11}$$

Symbol '*' stands for the space convolution defined by:

$$(f * g)(r) = \int_{V'} f(r-r')g(r')\,dV'.$$

By applying operator $\boldsymbol{\Pi^0}$ to Eq.(6), we obtain:

$$\boldsymbol{\Pi^0} * \boldsymbol{h}^0.\boldsymbol{q} = \boldsymbol{\Pi^0} * \boldsymbol{e} + \boldsymbol{\Pi^0} * \boldsymbol{h}^0.\delta\boldsymbol{k}.\boldsymbol{e}. \tag{12}$$

Using Eqs.(10) and (11), we obtain:

$$\boldsymbol{e} = \boldsymbol{e}^0 - \boldsymbol{\Pi^0} * \boldsymbol{h}^0.\delta\boldsymbol{k}.\boldsymbol{e}. \tag{13}$$

Eq. (13) may be expressed in the integral form as:

$$\boldsymbol{e}(\boldsymbol{r}) = \boldsymbol{e}^0 - \int_{V'} \boldsymbol{\Pi^0}(\boldsymbol{r}-\boldsymbol{r}').\boldsymbol{h}^0.\delta\boldsymbol{k}(\boldsymbol{r}').\boldsymbol{e}(\boldsymbol{r}')dV' \tag{14}$$

This integral equation provides the local intensity field for an arbitrary applied homogeneous intensity $\boldsymbol{e}^0$ and local anisotropic thermal conductivity. To solve this equation, the multi-coated inclusion model is then applied in the general case of arbitrary ellipsoidal morphology.

2.2. Multi-coated ellipsoidal inclusion

We consider a composite ellipsoidal inclusion that consists of a core with volume V_1, surrounded by *N-1* coatings. This composite inclusion is embedded in an HRM denoted '*0*' as matrix. The thermal conductivity is assumed anisotropic inside each phase and is described by second-order tensors $\boldsymbol{k}^P$, $P \in \{1,2,\dots,N\}$ and $\boldsymbol{k}^0$ for HRM. According to the topology of the multi-coated inclusion problem as depicted by Fig.1, the fluctuating part $\delta\boldsymbol{k}(\boldsymbol{r})$ of the local thermal conductivity $\boldsymbol{k}(\boldsymbol{r})$ is written as:

$$\delta\boldsymbol{k}(\boldsymbol{r}) = \sum_{P=1}^{N} \Delta\boldsymbol{k}^{P/0}\,\theta_P(\boldsymbol{r}) \quad \text{with} \quad \Delta\boldsymbol{k}^{P/0} = \boldsymbol{k}^P - \boldsymbol{k}^0 \tag{15}$$

where characteristic function $\theta_P(\boldsymbol{r})$ related to volume V_P of each phase '*P*' reads:

$$\theta_P(\boldsymbol{r}) = \begin{cases} 1 & \text{if } \boldsymbol{r} \in V_P \\ 0 & \text{if } \boldsymbol{r} \notin V_P \end{cases}.$$

In the following, the composite inclusion with volume Ω_N consists of the inclusion '*1*' and the $N-1$ coatings. For $J \in \{1,2,\dots,N\}$, Ω_J denotes the volume of the composite inclusion that is made with the inclusion '*1*' and the first $J-1$ coatings: $\Omega_N = \sum_{P=1}^{N} V_P$, $\Omega_J = \sum_{P=1}^{J} V_P$ and $V_P = \Omega_P - \Omega_{P-1}$. By substituting Eq.(15) in Eq.(14), we obtain:

$$\boldsymbol{e}(\boldsymbol{r}) = \boldsymbol{e}^0 - \sum_{P=1}^{N} \int_{V_P{}'} \boldsymbol{\Pi}^0(\boldsymbol{r}-\boldsymbol{r}').\boldsymbol{h}^0.\Delta\boldsymbol{k}^{P/0}.\boldsymbol{e}(\boldsymbol{r}')\, dV_P{}'. \tag{16}$$

Some volume averages of field $F(\boldsymbol{r})$, respectively inside the inclusion "1", a coating "P" and a composite inclusion Ω_J are then defined by:

$$\bar{F}^1 = \frac{1}{V_1}\int_{V_1} F(\boldsymbol{r})dV_1, \qquad \bar{F}^P = \frac{1}{V_P}\int_{V_P} F(\boldsymbol{r})dV_2 \quad \text{and} \quad \bar{F}^{\Omega_J} = \frac{1}{\Omega_J}\int_{\Omega_J} F(\boldsymbol{r})d\Omega_2. \tag{17}$$

These averages are related by $\bar{F}^{\Omega_J} = \frac{\Omega_N}{\Omega_J}\sum_{P=1}^{J}\phi_P\,\bar{F}^P$ where ϕ_P is the volume fraction of the phase "P" with volume V_P in the composite inclusion: $\phi_P = V_P/\Omega_N$ with $P \in \{1,2,\dots,N\}$. Thanks to Eq.(17), average of intensity inside composite inclusions Ω_N and Ω_J respectively results from:

$$\overline{\boldsymbol{e}}^{\Omega_N} = \sum_{P=1}^{N}\phi_P\,\overline{\boldsymbol{e}}^P \quad \text{and} \quad \overline{\boldsymbol{e}}^{\Omega_J} = \frac{\Omega_N}{\Omega_J}\sum_{P=1}^{J}\phi_P\,\overline{\boldsymbol{e}}^P$$

$\overline{\boldsymbol{e}}^P$ and $\overline{\boldsymbol{e}}^{\Omega_P}$ are then related by:

$$\phi_P\overline{\boldsymbol{e}}^P = \frac{\Omega_P}{\Omega_N}\,\overline{\boldsymbol{e}}^{\Omega_P} - \frac{\Omega_{P-1}}{\Omega_N}\,\overline{\boldsymbol{e}}^{\Omega_{P-1}}. \tag{18}$$

From Eq.(16), the average intensity inside the composite inclusion Ω_N reads:

$$\overline{\boldsymbol{e}}^{\Omega_N} = \boldsymbol{e}^0 - \frac{1}{\Omega_N}\sum_{P=1}^{N}\int_{\Omega_N}\int_{V_P{}'} \boldsymbol{\Pi}^0(\boldsymbol{r}-\boldsymbol{r}').\boldsymbol{h}^0.\Delta\boldsymbol{k}^{P/0}.\boldsymbol{e}(\boldsymbol{r}')\, dV_P{}'\, d\Omega_N. \tag{19}$$

The volume integral over the composite inclusion Ω_N is uniform since $\boldsymbol{r}' \in \Omega_N$ [16]. Thus, the interior-point Eshelby's conduction tensor $\boldsymbol{L}_0^{\Omega_N}$ associated to $\boldsymbol{k}^0$ and the ellipsoidal volume Ω_N is introduced as:

$$\boldsymbol{L}_0^{\Omega_N} = \int_{\Omega_N} \boldsymbol{\Pi}^0(\boldsymbol{r}-\boldsymbol{r}').\boldsymbol{h}^0\, d\Omega_N \quad \text{for} \quad \boldsymbol{r}' \in \Omega_N. \tag{20}$$

Eq.(19) becomes:

$$\overline{\boldsymbol{e}}^{\Omega_N} = \boldsymbol{e}^0 - \boldsymbol{L}_0^{\Omega_N}.\sum_{P=1}^{N}\phi_P\,\Delta\boldsymbol{k}^{P/0}.\overline{\boldsymbol{e}}^P. \tag{21}$$

Eq.(21) is exact, but for the expression of unknown intensities $\overline{\boldsymbol{e}}^{P}$ $(P = 1, 2, \dots, N)$, $N-1$ complementary equations have to be formulated. By proceeding similarly as previously, average intensity $\overline{\boldsymbol{e}}^{\Omega_J}$ inside composite inclusion Ω_J may be expressed from Eq.(14) as:

$$\begin{aligned}\overline{\boldsymbol{e}}^{\Omega_J} = \boldsymbol{e}^0 &- \frac{1}{\Omega_J}\sum_{P=1}^{J}\int_{\Omega_J}\int_{V_P{}'}\boldsymbol{\Pi}^0(\boldsymbol{r}-\boldsymbol{r}').\boldsymbol{h}^0.\Delta\boldsymbol{k}^{P/0}.\boldsymbol{e}(\boldsymbol{r}')\,dV_P{}'\,d\Omega_J \\ &- \frac{1}{\Omega_J}\sum_{P=J+1}^{N}\int_{\Omega_J}\int_{V_P{}'}\boldsymbol{\Pi}^0(\boldsymbol{r}-\boldsymbol{r}').\boldsymbol{h}^0.\Delta\boldsymbol{k}^{P/0}.\boldsymbol{e}(\boldsymbol{r}')\,dV_P{}'\,d\Omega_J.\end{aligned} \tag{22}$$

That is rewritten as:

$$\begin{aligned}\overline{\boldsymbol{e}}^{\Omega_J} = \boldsymbol{e}^0 &- \frac{1}{\Omega_J}\sum_{P=1}^{J}\int_{V_P{}'}\left\{\int_{\Omega_J}\boldsymbol{\Pi}^0(\boldsymbol{r}-\boldsymbol{r}').\boldsymbol{h}^0\,d\Omega_J\right\}.\Delta\boldsymbol{k}^{P/0}.\boldsymbol{e}(\boldsymbol{r}')dV_P{}' \\ &- \frac{1}{\Omega_J}\sum_{P=J+1}^{N}\int_{V_P{}'}\left\{\int_{\Omega_J}\boldsymbol{\Pi}^0(\boldsymbol{r}-\boldsymbol{r}').\boldsymbol{h}^0\,d\Omega_J\right\}.\Delta\boldsymbol{k}^{P/0}.\boldsymbol{e}(\boldsymbol{r}')dV_P{}'.\end{aligned} \tag{23}$$

In Eq.(23), the first double integral over Ω_J is uniform since $\boldsymbol{r}' \in V_P{}'$ as $\boldsymbol{r}'$ lies inside Ω_J [16].The uniform interior-point Eshelby's conduction tensor $\boldsymbol{L}_0^{\Omega_J}$ associated to $\boldsymbol{k}^0$ and the ellipsoidal volume Ω_J is therefore introduced as:

$$\boldsymbol{L}_0^{\Omega_J} = \int_{\Omega_J}\boldsymbol{\Pi}^0(\boldsymbol{r}-\boldsymbol{r}').\boldsymbol{h}^0\,d\Omega_J \quad \text{for} \quad \boldsymbol{r}' \in \Omega_J. \tag{24}$$

For the second double integral of Eq.(23), in absence of singularity one can permute the volume integrals over $V_P{}'$ and Ω_J as:

$$\begin{aligned}\overline{\boldsymbol{e}}^{\Omega_J} = \boldsymbol{e}^0 &- \frac{\Omega_N}{\Omega_J}\boldsymbol{L}_0^{\Omega_J}.\sum_{P=1}^{J}\phi_P\,\Delta\boldsymbol{k}^{P/0}.\overline{\boldsymbol{e}}^{\boldsymbol{p}} \\ &- \frac{1}{\Omega_J}\sum_{P=J+1}^{N}\int_{V_P{}'}\left\{\int_{\Omega_J}\boldsymbol{\Pi}^0(\boldsymbol{r}-\boldsymbol{r}').\boldsymbol{h}^0\,d\Omega_J\right\}.\Delta\boldsymbol{k}^{P/0}.\boldsymbol{e}(\boldsymbol{r}')dV_P{}'.\end{aligned} \tag{25}$$

The integral over the volume Ω_J in Eq.(25) is not uniform since $\boldsymbol{r}'$ is located outside the volume Ω_J. Furthermore, the intensity field $\boldsymbol{e}(\boldsymbol{r}')$ is also not uniform inside $V_P{}'$ due to strong interactions between local phases of the heterogeneous material. As a consequence, the exact expression of the integral term in Eq.(23) is difficult to obtain. Very few studies deal with this problem of multi-coated inclusions in a composite material. In elasticity, Hori and Nemat-Nasser [21] proposed a solution of the integral equation based on the assumption of the uniformity of strain field inside the coating. These authors therefore obtained simple but non-exact expressions of strain localization tensors. However, this model was extended to thermal conduction in heterogeneous materials [22-24].

Hereby, we propose a new formulation dealing with the exact solution of the multi-coated inclusion problem for anisotropic behavior per phase and ellipsoidal morphology.

2.3. New solution of the multi-coated inclusion problem

Classically, the integral formulation of heterogeneous problem is based on the Green's function technique associated to an arbitrary infinite HRM. In this section, we introduce an integral equation to complete Eq.(14). From Eq.(5), the local thermal conductivity $\boldsymbol{k}(\boldsymbol{r})$ is decomposed into a uniform part $\boldsymbol{k}^{J+1}$ of the coating *'J+1'* and fluctuating parts as:

$$\boldsymbol{k}(\boldsymbol{r}) = \boldsymbol{k}^{J+1} + \sum_{P=1}^{J} (\boldsymbol{k}^{P} - \boldsymbol{k}^{J+1})\theta_P(\boldsymbol{r}) + \sum_{P=J+2}^{N} (\boldsymbol{k}^{P} - \boldsymbol{k}^{J+1})\theta_P(\boldsymbol{r}) - (\boldsymbol{k}^{J+1} - \boldsymbol{k}^{0})\theta_0(\boldsymbol{r}). \tag{26}$$

The characteristic function $\theta_0(\boldsymbol{r})$ of the volume $V_0 = V - \Omega_N$ is defined by:

$\theta_0(\boldsymbol{r}) = 1 - \sum_{P=1}^{N} \theta_P(\boldsymbol{r})$ with $\boldsymbol{r} \in V_0$.

Thanks to Eq.(26), Eq.(6) becomes:

$$q(\boldsymbol{r}) = \boldsymbol{k}^{J+1}.\boldsymbol{e}(\boldsymbol{r}) + \sum_{P=1}^{J} \Delta\boldsymbol{k}^{P/(J+1)}.\boldsymbol{e}(\boldsymbol{r})\,\theta_P(\boldsymbol{r}) + \sum_{P=J+2}^{N} \Delta\boldsymbol{k}^{P/(J+1)}.\boldsymbol{e}(\boldsymbol{r})\,\theta_P(\boldsymbol{r}) - \Delta\boldsymbol{k}^{J+1/0}.\boldsymbol{e}(\boldsymbol{r})\theta_0(\boldsymbol{r}). \tag{27}$$

In light of the decomposition Eq.(26), we introduce a Green's function G^{J+1} associated to thermal conductivity $\boldsymbol{k}^{J+1}$ that vanishes at infinity but still finite at boundaries of the volume V_{J+1} as:

$$k_{ij}^{J+1}\frac{\partial^2 G^{J+1}(\boldsymbol{r}-\boldsymbol{r}')}{\partial x_i\,\partial x_j}+\delta(\boldsymbol{r}-\boldsymbol{r}')=0 \quad \text{and} \quad \lim_{|\boldsymbol{r}-\boldsymbol{r}'|\to\infty} G^{J+1}(\boldsymbol{r}-\boldsymbol{r}')=0. \tag{28}$$

A projection operator $\boldsymbol{\Pi}^{J+1}$ associated to $\boldsymbol{k^{J+1}}$ is then defined by:

$$\boldsymbol{\Pi}^{J+1}=\boldsymbol{\Gamma}^{J+1}.\boldsymbol{k}^{J+1} \tag{29}$$

and related to modified Green's tensor $\boldsymbol{\Gamma}^{J+1}$ as:

$$\boldsymbol{\Gamma}^{J+1}=-\boldsymbol{\nabla}\boldsymbol{\nabla}G^{J+1}. \tag{30}$$

$\boldsymbol{\Pi}^{J+1}$ has same properties as $\boldsymbol{\Pi}^{0}$:

$$\boldsymbol{e}=-\boldsymbol{\nabla}T \text{ and } T=-\boldsymbol{e}^0.\boldsymbol{r} \quad \text{on} \quad \partial V \;\Leftrightarrow \boldsymbol{\Pi}^{J+1}*\boldsymbol{e}=\boldsymbol{e}-\boldsymbol{e}^0; \tag{31}$$

$$div\boldsymbol{q}=0 \Leftrightarrow \boldsymbol{\Pi}^{J+1}*\boldsymbol{h}^{J+1}.\boldsymbol{q}=0 \quad \text{with} \quad \boldsymbol{h}^{J+1}=\boldsymbol{k}^{J+1^{-1}}. \tag{32}$$

Using Eqs.(31) and (32), we obtain a new integral equation as:

$$\begin{aligned}\boldsymbol{e}(\boldsymbol{r})=\boldsymbol{e}^0&-\sum_{P=1}^{J}\int_{V_P{}'}\boldsymbol{\Pi}^{J+1}(\boldsymbol{r}-\boldsymbol{r}').\boldsymbol{h}^{J+1}.\Delta\boldsymbol{k}^{P/J+1}.\boldsymbol{e}(\boldsymbol{r}')\,dV_P{}'\\&-\sum_{P=J+2}^{N}\int_{V_P{}'}\boldsymbol{\Pi}^{J+1}(\boldsymbol{r}-\boldsymbol{r}').\boldsymbol{h}^{J+1}.\Delta\boldsymbol{k}^{P/J+1}.\boldsymbol{e}(\boldsymbol{r}')\,dV_P{}'\\&+\int_{V_0{}'}\boldsymbol{\Pi}^{J+1}(\boldsymbol{r}-\boldsymbol{r}').\boldsymbol{h}^{J+1}.\Delta\boldsymbol{k}^{J+1/0}.\boldsymbol{e}(\boldsymbol{r}')\,dV_0{}'.\end{aligned} \tag{33}$$

From Eq.(33), the volume average $\overline{\boldsymbol{e}}^{\Omega_J}$ inside the composite inclusion Ω_J reads:

$$\overline{\boldsymbol{e}}^{\Omega_J} = \boldsymbol{e}^0 - \frac{1}{\Omega_J}\sum_{P=1}^{J}\int_{V_P{}'}\left\{\int_{\Omega_J}\boldsymbol{\Pi}^{J+1}(\boldsymbol{r}-\boldsymbol{r}').\boldsymbol{h}^{J+1}\,d\Omega_J\right\}.\Delta\boldsymbol{k}^{P/J+1}.\boldsymbol{e}(\boldsymbol{r}')dV_P{}'$$

$$-\frac{1}{\Omega_J}\sum_{P=J+2}^{N}\int_{V_P{}'}\left\{\int_{\Omega_J}\boldsymbol{\Pi}^{J+1}(\boldsymbol{r}-\boldsymbol{r}').\boldsymbol{h}^{J+1}\,d\Omega_J\right\}.\Delta\boldsymbol{k}^{P/J+1}.\boldsymbol{e}(\boldsymbol{r}')dV_P{}' \tag{34}$$

$$+\frac{1}{\Omega_J}\int_{V_0{}'}\left\{\int_{\Omega_J}\boldsymbol{\Pi}^{J+1}(\boldsymbol{r}-\boldsymbol{r}').\boldsymbol{h}^{J+1}\,d\Omega_J\right\}.\Delta\boldsymbol{k}^{J+1/0}.\boldsymbol{e}(\boldsymbol{r}')dV_0{}'.$$

In Eq.(34), the volume integral over Ω_J is uniform if $\boldsymbol{r}' \in \Omega_J$ and a interior-point Eshelby's conduction tensor $\boldsymbol{L}_{J+1}^{\Omega_J}$ associated to $\boldsymbol{k}^{J+1}$ and the ellipsoidal volume Ω_J is introduced as:

$$\boldsymbol{L}_{J+1}^{\Omega_J} = \int_{\Omega_J}\boldsymbol{\Pi}^{J+1}(\boldsymbol{r}-\boldsymbol{r}').\boldsymbol{h}^{J+1}\,d\Omega_J \quad \text{for} \quad \boldsymbol{r}' \in \Omega_J. \tag{35}$$

But for $\boldsymbol{r}' \notin \Omega_J$, the volume integral over Ω_J is not uniform. In this case, an exterior-point Eshelby's conduction tensor $\boldsymbol{L}_{J+1}^{Ext/\Omega_J}(\boldsymbol{r}')$ is considered:

$$L_{J+1}^{Ext/\Omega_J}(\boldsymbol{r}') = \int_{\Omega_J}\boldsymbol{\Pi}^{J+1}(\boldsymbol{r}-\boldsymbol{r}').\boldsymbol{h}^{J+1}\,d\Omega_J \quad \text{for} \quad \boldsymbol{r}' \notin \Omega_J. \tag{36}$$

Using Eqs.(35) and (36), Eq.(34) is rewritten as:

$$\overline{\boldsymbol{e}}^{\Omega_J} = \boldsymbol{e}^0 - \frac{\Omega_N}{\Omega_J}\,\boldsymbol{L}_{J+1}^{\Omega_J}.\sum_{P=1}^{J}\phi_P\,\Delta\boldsymbol{k}^{P/J+1}.\overline{\boldsymbol{e}}^P$$

$$-\frac{1}{\Omega_J}\sum_{P=J+2}^{N}\int_{V_P{}'}\boldsymbol{L}_{J+1}^{Ext/\Omega_J}(\boldsymbol{r}').\Delta\boldsymbol{k}^{P/J+1}.\boldsymbol{e}(\boldsymbol{r}')\,dV_P{}' \tag{37}$$

$$+\frac{1}{\Omega_J}\int_{V_0{}'}\boldsymbol{L}_{J+1}^{Ext/\Omega_J}(\boldsymbol{r}').\Delta\boldsymbol{k}^{J+1/0}.\boldsymbol{e}(\boldsymbol{r}')\,dV_0{}'.$$

Similarly, $\overline{\boldsymbol{e}}^{\Omega_{J+1}}$ reads:

$$\overline{\boldsymbol{e}}^{\Omega_{J+1}} = \boldsymbol{e}^0 - \frac{\Omega_N}{\Omega_{J+1}} \boldsymbol{L}_{J+1}^{\Omega_{J+1}} . \sum_{P=1}^{J} \phi_P \, \Delta \boldsymbol{k}^{P/J+1} . \overline{\boldsymbol{e}}^P$$

$$- \frac{1}{\Omega_{J+1}} \sum_{P=J+2}^{N} \int_{V_P'} \boldsymbol{L}_{J+1}^{Ext/\Omega_{J+1}}(\boldsymbol{r}') . \Delta \boldsymbol{k}^{P/J+1} . \boldsymbol{e}(\boldsymbol{r}') \, dV_P' \tag{38}$$

$$+ \frac{1}{\Omega_{J+1}} \int_{V_0'} \boldsymbol{L}_{J+1}^{Ext/\Omega_{J+1}}(\boldsymbol{r}') . \Delta \boldsymbol{k}^{J+1/0} . \boldsymbol{e}(\boldsymbol{r}') \, dV_0' .$$

Then, the difference between $\overline{\boldsymbol{e}}^{\Omega_J}$ and $\overline{\boldsymbol{e}}^{\Omega_{J+1}}$ is obtained as:

$$\overline{\boldsymbol{e}}^{\Omega_{J+1}} - \overline{\boldsymbol{e}}^{\Omega_J} = \frac{V_{J+1}}{\Omega_J} \frac{\Omega_N}{\Omega_{J+1}} \boldsymbol{L}_{J+1}^{J+1} . \sum_{P=1}^{J} \phi_P \, \Delta \boldsymbol{k}^{P/J+1} . \overline{\boldsymbol{e}}^P$$

$$- \frac{1}{\Omega_J} \sum_{P=J+2}^{N} \int_{V_P'} \boldsymbol{\Lambda}_{J+1}^{Ext/\Omega_{J+1}-\Omega_J}(\boldsymbol{r}') . \Delta \boldsymbol{k}^{P/J+1} . \boldsymbol{e}(\boldsymbol{r}') \, dV_P' \tag{39}$$

$$+ \frac{1}{\Omega_J} \int_{V_0'} \boldsymbol{\Lambda}_{J+1}^{Ext/\Omega_{J+1}-\Omega_J}(\boldsymbol{r}') . \Delta \boldsymbol{k}^{J+1/0} . \boldsymbol{e}(\boldsymbol{r}') \, dV_0' .$$

where

$$L_{J+1}^{J+1} = \boldsymbol{L}_{J+1}^{\Omega_{J+1}} - \frac{\Omega_{J+1}}{V_{J+1}} \left(\boldsymbol{L}_{J+1}^{\Omega_{J+1}} - \boldsymbol{L}_{J+1}^{\Omega_J} \right) ; \tag{40}$$

$$\boldsymbol{\Lambda}_{J+1}^{Ext/\Omega_{J+1}-\Omega_J}(\boldsymbol{r}') = \boldsymbol{L}_{J+1}^{Ext/\Omega_J}(\boldsymbol{r}') - \frac{\Omega_J}{\Omega_{J+1}} \boldsymbol{L}_{J+1}^{Ext/\Omega_{J+1}}(\boldsymbol{r}'). \tag{41}$$

Integral terms in Eq.(39) are difficult to evaluate since the tensor $\boldsymbol{\Lambda}_{J+1}^{Ext/\Omega_{J+1}-\Omega_J}(\boldsymbol{r}')$ are not uniform in volume V_0' exterior to Ω_J and Ω_{J+1}. Moreover, local intensity field $\boldsymbol{e}(\boldsymbol{r}')$ is also not uniform in the volume V_0'. Since $\boldsymbol{L}_{J+1}^{Ext/\Omega_J}(\boldsymbol{r}')$ and $\boldsymbol{L}_{J+1}^{Ext/\Omega_{J+1}}(\boldsymbol{r}')$ depend on the morphology of ellipsoids Ω_J and Ω_{J+1} respectively and Green's function G^{J+1} associated to $\boldsymbol{k}^{J+1}$, we propose hereafter to express tensor $\boldsymbol{\Lambda}_{J+1}^{Ext/\Omega_{J+1}-\Omega_J}(\boldsymbol{r}')$.

2.4. Expressions of tensors $\boldsymbol{L}_{J+1}^{Ext/\Omega_J}(\boldsymbol{r}')$ and $\boldsymbol{L}_{J+1}^{Ext/\Omega_{J+1}}(\boldsymbol{r}')$ *for anisotropic thermal conductivity*

Using Eqs.(29) and(30), exterior-point Eshelby's conduction tensor $\boldsymbol{L}_{J+1}^{Ext/\Omega_P}(\boldsymbol{r}')$ as defined by Eq.(36) may be expressed in terms of Green's conduction function G^{J+1} :

$$L_{J+1_{im}}^{Ext/\Omega_p}(\boldsymbol{r}') = -\int_{\Omega_p} \frac{\partial^2 G^{J+1}(\boldsymbol{r}-\boldsymbol{r}')}{\partial x_i\, \partial x_m} d\Omega_p \quad \text{for} \quad \boldsymbol{r}' \notin \Omega_p \text{ and } P \in \{J, J+1\}\,. \tag{42}$$

When the tensor $\boldsymbol{k}^{J+1}$ is anisotropic, the computation of Eq.(39) is difficult to achieve. By assuming the thermal conductivity to orthotropic, $\boldsymbol{k}^{J+1}$ is written as:

$$\boldsymbol{k}^{J+1} = \begin{pmatrix} k_1^{J+1} & 0 & 0 \\ 0 & k_2^{J+1} & 0 \\ 0 & 0 & k_3^{J+1} \end{pmatrix}, \; J = 1,2,\ldots,N-1.$$

Green function G^{J+1} arises from the solution of the differential equation Eq.(28). Following an approach proposed by Giordano [28], the tensor $\boldsymbol{k}^{J+1}$ is rendered isotropic through a linear transformation of Cartesian coordinates. The following linear transformation of Cartesian coordinates transforms the vector position $\boldsymbol{r}(x_1, x_2, x_3)$ into the vector $\boldsymbol{y}(y_1, y_2, y_3)$ through:

$$y_i = \frac{x_i}{\gamma_i^{J+1}} \quad \text{and} \quad \gamma_i^{J+1}\frac{\partial}{\partial x_i} = \frac{\partial}{\partial y_i} \quad \text{with} \quad \gamma_i^{J+1} = \sqrt{\frac{k_i^{J+1}}{k_1^{J+1}}}. \tag{43}$$

Eq.(28) may then be rewritten as:

$$\gamma_1^{J+1}\,\gamma_2^{J+1}\,\gamma_3^{J+1}\,k_1^{J+1}\,\frac{\partial^2 \tilde{G}^{J+1}(\boldsymbol{y}-\boldsymbol{y}')}{\partial y_p\, \partial y_p} + \tilde{\delta}(\boldsymbol{y}-\boldsymbol{y}') = 0 \quad \text{and} \quad \lim_{|\boldsymbol{y}-\boldsymbol{y}'|\to\infty} \tilde{G}^{J+1}(\boldsymbol{y}-\boldsymbol{y}') = 0\,. \tag{44}$$

where $G^{J+1}(\boldsymbol{r})$ is the transformed into $\tilde{G}^{J+1}(\boldsymbol{y})$. Eq.(44) may be solved to provide the transformed Green's conduction function $\tilde{G}^{J+1}$:

$$\tilde{G}^{J+1}(\boldsymbol{y}-\boldsymbol{y}') = \frac{1}{4\,\pi\,\gamma_1^{J+1}\,\gamma_2^{J+1}\,\gamma_3^{J+1}\,k_1^{J+1}}\frac{1}{|\boldsymbol{y}-\boldsymbol{y}'|}. \tag{45}$$

Ellipsoids Ω_{J} and $\Omega_{\mathrm{J+1}}$ with semi-axes a_i^J and a_i^{J+1} $(i = 1, 2, 3)$ are then transformed into the ellipsoids $\widetilde{\Omega}_{\mathrm{J}}$ and $\widetilde{\Omega}_{\mathrm{J+1}}$ with semi-axes $\tilde{a}_i^J$ and $\tilde{a}_i^{J+1}$ through : $\tilde{a}_i^J = a_i^J/\gamma_i^{J+1}$ and $\tilde{a}_i^{J+1} = a_i^{J+1}/\gamma_i^{J+1}$.

The ellipsoidal volume Ω_J and surface S_J is surrounded by a coating V_{J+1}. The corresponding composite inclusion has the volume $\Omega_{\mathrm{J+1}}$ and external surface S_{J+1}.

$$\sum_{i=1}^{3} \frac{x_i^2}{\left(\tilde{a}_i^J\right)^2} = 1 \quad \text{for} \quad x \in S_J \; ; \quad \sum_{i=1}^{3} \frac{x_i^2}{\left(\tilde{a}_i^{J+1}\right)^2} = 1 \quad \text{for} \quad x \in S_{J+1}. \tag{46}$$

Similarly, external surfaces S_J and S_{J+1} are also transformed into $\tilde{S}_J$ and $\tilde{S}_{J+1}$ respectively defined by:

$$\sum_{i=1}^{3} \frac{y_i^2}{\left(\tilde{a}_i^J\right)^2} = 1 \quad \text{for} \quad \boldsymbol{y} \in \tilde{S}_J \; ; \quad \sum_{i=1}^{3} \frac{y_i^2}{\left(\tilde{a}_i^{J+1}\right)^2} = 1 \quad \text{for} \quad \boldsymbol{y} \in \tilde{S}_{J+1}. \tag{47}$$

$\boldsymbol{L}_{J+1}^{Ext/\Omega_{\mathrm{P}}}(\boldsymbol{r}')$ as defined by Eq.(36) becomes:

$$L_{J+1_{im}}^{Ext/\Omega_P}(\boldsymbol{r}') = -\frac{1}{4\,\pi\, k_{nm}^{J+1}\, \gamma_i^{J+1}\, \gamma_n^{J+1}} \frac{\partial^2}{\partial y_i'\, \partial y_n'} \int_{\widetilde{\Omega}_P} \frac{1}{|\boldsymbol{y} - \boldsymbol{y}'|}\, d\widetilde{\Omega}_P \quad \text{for} \quad \boldsymbol{y}' \notin \widetilde{\Omega}_P. \tag{48}$$

Let us introduce harmonic functions $\tilde{\varphi}^{Ext/\Omega_{\mathrm{J}}}$ for $J \in \{1,2, \ldots, N\}$ as defined in [29]:

$$\tilde{\varphi}^{Ext/\Omega_P}(\boldsymbol{y}') = \int_{\widetilde{\Omega}_J} \frac{1}{|\boldsymbol{y} - \boldsymbol{y}'|}\, d\widetilde{\Omega}_P \quad \text{for} \quad \boldsymbol{y}' \notin \widetilde{\Omega}_P. \tag{49}$$

Then, Eq.(48) read as:

$$L_{J+1_{im}}^{Ext/\Omega_P}(\boldsymbol{r}') = \frac{-1}{4\,\pi\, k_{nm}^{J+1}\, \gamma_i^{J+1}\, \gamma_n^{J+1}} \frac{\partial^2 \tilde{\varphi}^{Ext/\Omega_P}(\boldsymbol{y}')}{\partial y_i'\, \partial y_n'}. \tag{50}$$

Expressions of harmonic functions $\tilde{\varphi}^{Ext/\Omega_{\mathrm{J}}}$ and $\tilde{\varphi}^{Ext/\Omega_{\mathrm{J+1}}}$ are provided in [29]:

$$\begin{aligned} \tilde{\varphi}^{Ext/\Omega_{\mathrm{J}}}(\boldsymbol{y}') &= \frac{1}{2}\left(\tilde{I}\left(\tilde{a}_i^J, \tilde{\lambda}_1\right) - y_n'\, y_n'\, \tilde{I}_n\left(\tilde{a}_i^J, \tilde{\lambda}_1\right)\right); \\ \tilde{\varphi}^{Ext/\Omega_{J+1}}(\boldsymbol{y}') &= \frac{1}{2}\left(\tilde{I}\left(\tilde{a}_i^{J+1}, \tilde{\lambda}_2\right) - y_n'\, y_n'\, \tilde{I}_n\left(\tilde{a}_i^{J+1}, \tilde{\lambda}_2\right)\right) \end{aligned} \tag{51}$$

where $\tilde{I}$ and $\tilde{I}_n$ are *I*-elliptic integrals defined by:

$$\tilde{I}\left(\tilde{a}_i^J, \tilde{\lambda}_J\right) = 2\,\pi\,\tilde{a}_1^J\,\tilde{a}_2^J\,\tilde{a}_3^J \int_{\tilde{\lambda}_J}^{\infty} \frac{ds}{\Delta_1(s)};$$

$$\tilde{I}_n\left(\tilde{a}_i^J, \tilde{\lambda}_J\right) = 2\,\pi\,\tilde{a}_1^J\,\tilde{a}_2^J\,\tilde{a}_3^J \int_{\tilde{\lambda}_J}^{\infty} \frac{ds}{\left(\left(\tilde{a}_n^J\right)^2 + s\right)\Delta_1(s)};$$

$$\tilde{I}\left(\tilde{a}_i^{J+1}, \tilde{\lambda}_{J+1}\right) = 2\,\pi\,\tilde{a}_1^{J+1}\,\tilde{a}_2^{J+1}\,\tilde{a}_3^{J+1} \int_{\tilde{\lambda}_{J+1}}^{\infty} \frac{ds}{\Delta_2(s)}; \tag{52}$$

$$\tilde{I}_n\left(\tilde{a}_i^{J+1}, \tilde{\lambda}_{J+1}\right) = 2\,\pi\,\tilde{a}_1^{J+1}\,\tilde{a}_2^{J+1}\,\tilde{a}_3^{J+1} \int_{\tilde{\lambda}_{J+1}}^{\infty} \frac{ds}{\left(\left(\tilde{a}_n^{J+1}\right)^2 + s\right)\Delta_2(s)}$$

with

$$\Delta_1(s) = \left(\left(\left(\tilde{a}_1^J\right)^2 + s\right)\left(\left(\tilde{a}_2^J\right)^2 + s\right)\left(\left(\tilde{a}_3^J\right)^2 + s\right)\right)^{1/2};$$

$$\Delta_2(s) = \left(\left(\left(\tilde{a}_1^{J+1}\right)^2 + s\right)\left(\left(\tilde{a}_2^{J+1}\right)^2 + s\right)\left(\left(\tilde{a}_3^{J+1}\right)^2 + s\right)\right)^{1/2}.$$

The variables $\tilde{\lambda}_J$ and $\tilde{\lambda}_{J+1}$ are defined by:

$$\sum_{i=1}^{3} \frac{y_i'^2}{\left(\tilde{a}_i^J\right)^2 + \tilde{\lambda}_J} = 1 \quad \text{and} \quad \sum_{i=1}^{3} \frac{y_i'^2}{\left(\tilde{a}_i^{J+1}\right)^2 + \tilde{\lambda}_{J+1}} = 1. \tag{53}$$

Since ellipsoids $\widetilde{\Omega}_{\mathrm{J}}$ and $\widetilde{\Omega}_{\mathrm{J+1}}$ are assumed confocal, following relations hold true:

$$\left(\tilde{a}_3^{J+1}\right)^2 - \left(\tilde{a}_1^{J+1}\right)^2 = \left(\tilde{a}_3^J\right)^2 - \left(\tilde{a}_1^J\right)^2 \quad \text{and} \quad \left(\tilde{a}_3^{J+1}\right)^2 - \left(\tilde{a}_2^{J+1}\right)^2 = \left(\tilde{a}_3^J\right)^2 - \left(\tilde{a}_2^J\right)^2$$

that may be rewritten thanks to Eq.(53) as:

$$\left(\tilde{a}_i^{J+1}\right)^2 + \tilde{\lambda}_{J+1} = \left(\tilde{a}_i^J\right)^2 + \tilde{\lambda}_J \text{ for } i \in \{1,2,3\}.$$

I-elliptic integrals in Eq.(52) are then related by:

$$\frac{1}{\widetilde{\Omega}_{\mathrm{J}}}\tilde{I}\left(\tilde{a}_i^J, \tilde{\lambda}_{\mathrm{J}}\right) = \frac{1}{\widetilde{\Omega}_{\mathrm{J+1}}}\tilde{I}\left(\tilde{a}_i^{J+1}, \tilde{\lambda}_{\mathrm{J+1}}\right) \text{ and } \frac{1}{\widetilde{\Omega}_{\mathrm{J}}}\tilde{I}_n\left(\tilde{a}_i^J, \tilde{\lambda}_{\mathrm{J}}\right) = \frac{1}{\widetilde{\Omega}_{\mathrm{J+1}}}\tilde{I}_n\left(\tilde{a}_i^{J+1}, \tilde{\lambda}_{\mathrm{J+1}}\right).$$

In light of Eq.(51), one obtains:

$$\frac{1}{\widetilde{\Omega}_{\mathrm{J}}}\tilde{\varphi}^{Ext/\Omega_{\mathrm{J}}}(\boldsymbol{y}') = \frac{1}{\widetilde{\Omega}_{\mathrm{J+1}}}\tilde{\varphi}^{Ext/\Omega_{\mathrm{J+1}}}(\boldsymbol{y}').$$

and finally:

$$L^{Ext/\Omega_P}_{J+1_{nn}}(\boldsymbol{r}') = \frac{1}{4\,\pi\,k^{J+1}_{nn}}\tilde{I}_n\left(\tilde{a}^P_i, \tilde{\lambda}_P\right), \;\; P = J, J+1. \tag{54}$$

The interior-point Eshelby's conduction tensor ($\tilde{\lambda}_P = 0$) reads:

$$L^{\Omega_P}_{J+1_{nn}} = \frac{1}{4\,\pi\,k^{J+1}_{nn}}\tilde{I}_n(\tilde{a}^P_i, 0), \quad P = J, J+1. \tag{55}$$

and:

$$L^{\Omega_N}_{0_{nn}} = \frac{1}{4\,\pi\,k^{0}_{nn}}\tilde{I}_n(\tilde{a}^N_i, 0). \tag{56}$$

Moreover, since $\widetilde{\Omega}_{\mathrm{J}}/\widetilde{\Omega}_{\mathrm{J+1}} = \Omega_{\mathrm{J}}/\Omega_{\mathrm{J+1}}$, $\boldsymbol{L}^{Ext/\Omega_{\mathrm{J}}}_{J+1}(\boldsymbol{r}')$ and $\boldsymbol{L}^{Ext/\Omega_{\mathrm{J+1}}}_{J+1}(\boldsymbol{r}')$ are related by:

$$\frac{1}{\Omega_J}\boldsymbol{L}^{Ext/\Omega_J}_{J+1}(\boldsymbol{r}') = \frac{1}{\Omega_{J+1}}\boldsymbol{L}^{Ext/\Omega_{J+1}}_{J+1}(\boldsymbol{r}'). \tag{57}$$

Consequently, from Eq.(57) we obtain:

$$\boldsymbol{\Lambda}^{Ext/\Omega_{J+1}-\Omega_J}_{J+1}(\boldsymbol{r}') = 0. \tag{58}$$

Eq.(39) is then reduced to:

$$\overline{\boldsymbol{e}}^{\Omega_{\mathrm{J+1}}} - \overline{\boldsymbol{e}}^{\Omega_{\mathrm{J}}} = \frac{V_{J+1}}{\Omega_J}\frac{\Omega_N}{\Omega_{J+1}}\boldsymbol{L}^{J+1}_{J+1}.\sum_{P=1}^{J}\phi_P\,\Delta\boldsymbol{k}^{P/J+1}.\overline{\boldsymbol{e}}^{P}. \tag{59}$$

Local intensity $\overline{\boldsymbol{e}}^{J+1}$ is obtained through a recursive procedure:

$$\overline{\boldsymbol{e}}^{J+1} = \frac{1}{\sum_{P=1}^{J}\phi_P}\sum_{P=1}^{J}\phi_P\left(\boldsymbol{I} + \boldsymbol{L}^{J+1}_{J+1}.\Delta\boldsymbol{k}^{P/J+1}\right).\overline{\boldsymbol{e}}^{P}, \qquad \text{for } \; J \in \{1,2,\dots,N-1\} \tag{60}$$

Furthermore, Eq.(21) is recasted as:

$$\sum_{P=1}^{N}\phi_P\left(\boldsymbol{I} + \boldsymbol{L}^{\Omega_{\mathrm{N}}}_{0}.\Delta\boldsymbol{k}^{P/0}\right).\overline{\boldsymbol{e}}^{P} = \boldsymbol{e}^0 \tag{61}$$

The system of Eqs.(60) and (61) provide the solution in terms of volume average intensity inside each phase of the composite inclusion as function of the imposed intensity $\boldsymbol{e}^0$. The resolution of this

system of equations constitutes the solution of the problem of multicoated inclusion without any assumption.

The effective thermal conductivity of heterogeneous material can then be predicted through classical homogenization schemes such as Generalized Mori Tanaka or Generalized Self-Consistent (GSC).

3. Effective thermal conductivity

We consider a *N*-phase composite made of multi-coated ellipsoidal inclusions embedded in a matrix. All the interfaces between the phases are considered perfect.

Macroscopic heat flux $\boldsymbol{Q}$ and intensity $\boldsymbol{E}$ of the composite read:

$$\begin{aligned} \boldsymbol{E} &= -\frac{1}{V}\int_{\partial V} T(\boldsymbol{r})\,\boldsymbol{n}\,dS = \frac{1}{V}\int_{V} \boldsymbol{e}(\boldsymbol{r})\,dV; \\ \boldsymbol{Q} &= \frac{1}{V}\int_{\partial V} \boldsymbol{q}(\boldsymbol{r}).\boldsymbol{n}\,\boldsymbol{r}dS = \frac{1}{V}\int_{V} \boldsymbol{q}(\boldsymbol{r})\,dV. \end{aligned} \tag{62}$$

$\boldsymbol{n}$ is the outward unit vector normal to the boundary ∂V of the volume V of RVE.

Macroscopic fields $\boldsymbol{Q}$ and $\boldsymbol{E}$ are related by the effective thermal conductivity $\boldsymbol{k}^{eff}$:

$$\boldsymbol{Q} = \boldsymbol{k}^{eff}.\boldsymbol{E} \tag{63}$$

The solution of the system of Eqs.(60) and (70) gives the localizationof the average intensity inside each phase :

$$\overline{\boldsymbol{e}}^{P} = \boldsymbol{A}^{P}.\boldsymbol{E} \quad \text{with} \quad \sum_{P=1}^{N} f_P\,\boldsymbol{A}^{P} = \boldsymbol{I}. \tag{64}$$

$\boldsymbol{A}^{P}$ is the intensity localizationtensor inside the phase '*P*' and $\boldsymbol{I}$ the second-order identity tensor.

The effective thermal conductivity is expressed as:

$$\boldsymbol{k}^{eff} = \sum_{P=1}^{N} f_P\,\boldsymbol{k}^{P}.\boldsymbol{A}^{P} \tag{65}$$

where the volume fraction of the phase 'P' is defined by $f_P = V_P/V$. Analytical expressions of localization tensors $\boldsymbol{A}^P$ and effective thermal conductivity tensors $\boldsymbol{k}^{eff}$ are therefore deduced through two homogenization schemes.

3.1. Generalized Mori Tanaka scheme

Mori-Tanaka model has been formulated by Mori-Tanaka [30] for the prediction of effective properties of two-phase composite materials. This model is based on the concept of Eshelby's inclusion [4], assuming that an ellipsoidal inclusion is embedded inside a matrix. The topology of Mori-Tanaka model assumes that the HRM introduced for the integral equation is subjected at its boundary to the same strain field as the matrix. Mori-Tanaka model provides simple analytical solution and is easy to implement. This model is generalized here to the case multi-coated inclusions in heterogeneous materials. In Eq.(60) by putting $\boldsymbol{k}^0 = \boldsymbol{k}^M$ and $\boldsymbol{e}^0 = \boldsymbol{e}^M$, we obtain:

$$\overline{\boldsymbol{e}}^{J+1} = \frac{1}{\sum_{P=1}^{J} \phi_P} \sum_{P=1}^{J} \phi_P \left(\boldsymbol{I} + \boldsymbol{L}_{J+1}^{J+1}.\Delta\boldsymbol{k}^{P/J+1}\right).\overline{\boldsymbol{e}}^P, \qquad \text{for } J \in \{1,2,\dots,N-1\}$$
$$\sum_{P=1}^{N} \phi_P \left(\boldsymbol{I} + \boldsymbol{L}_M^{\Omega_N}.\Delta\boldsymbol{k}^{P/M}\right).\overline{\boldsymbol{e}}^P = \boldsymbol{e}^M \tag{66}$$

Mean fields of local intensity inside each phase of the VER are then expressed as : $\overline{\boldsymbol{e}}^P = \boldsymbol{A}^{P/M}.\overline{\boldsymbol{e}}^M$. Then thanks to Eq.(62) we obtain:

$$\overline{\boldsymbol{e}}^{\boldsymbol{M}} = \boldsymbol{A}^M.\boldsymbol{E}, \quad \text{where} \quad \boldsymbol{A}^M = \left(f_M + \sum_{P=1}^{N-1} f_P\, \boldsymbol{A}^{P/M}\right)^{-1} \tag{67}$$

so that:

$$\overline{\boldsymbol{e}}^{\boldsymbol{P}} = \boldsymbol{A}^P.\boldsymbol{E} \quad \text{with} \quad \boldsymbol{A}^P = \boldsymbol{A}^{P/M}.\boldsymbol{A}^M \quad \text{for} \quad P = 1,2,\dots,N-1 \tag{68}$$

The effective thermal conductivity is then deduced from Eq.(65).

3.2. Generalized Self-Consistent scheme

GSC scheme was first introduced by Hashin [11] for a two-phase material from the solution of a coated spherical inclusion embedded in an HEM by considering an isotropic thermal conductivity per phase. This model was extended to multi-coated spherical inclusion [12]. In the present section, the GSC scheme is developed in the general case of multi-coated ellipsoidal inclusion and anisotropic thermal conductivity per phase. Within the framework of GSC scheme, the composite inclusion Ω_N is assumed embedded in HEM. The solution of the multi-coated problem is acquired through Eqs.(60) and (61) by replacing the reference medium denoted '0' by the HEM denoted by 'eff':

$$\boldsymbol{e}^0 = \boldsymbol{E} \quad \text{and} \quad \boldsymbol{k}^0 = \boldsymbol{k}^{eff}. \tag{69}$$

Thanks to Eq.(69), Eq.(21) is reduced to:

$$\overline{\boldsymbol{e}}^{\Omega_N} = \boldsymbol{E}. \tag{70}$$

The solution of the system of Eqs.(60) and (70) gives the localizationof the average intensity inside each phase as :

$$\overline{\boldsymbol{e}}^{P} = \boldsymbol{A}^{P}.\boldsymbol{E} \quad \text{with} \quad \sum_{P=1}^{N} f_P \, \boldsymbol{A}^{P} = \boldsymbol{I}. \tag{71}$$

The effective thermal conductivity is then provided by Eq.(65).

It's worth mentioning that, contrary to classical GSC scheme that provides the effective properties through an iterative process, the present formulation leads to explicit analytical expression of $\boldsymbol{k}^0 = \boldsymbol{k}^{eff}$ (without iteration), even for ellipsoidal inclusions and anisotropic thermal conductivity per phase.

4. Applications

4.1. Simply coated inclusion ($N = 2$)

Let us consider an ellipsoidal inclusion with semi-axis a_1, a_2 and a_3, of volume V_1 surrounded by the interphase of volume V_2 (Fig.2). The corresponding composite ellipsoidal inclusion with volume $\Omega_2 = V_1 + V_2$ and semi-axis b_1, b_2, b_3 is embedded in an infinite HRM denoted '*0*'. The anisotropic

thermal conductivity of each phase is described by tensor $\boldsymbol{k}^1$, $\boldsymbol{k}^2$ and $\boldsymbol{k}^0$ for the inclusion, the interphase and the HRM, respectively. By solving the system of Eqs.(60) and (70), localization of intensity inside the inclusion and the interphase are given by:

$$\overline{\boldsymbol{e}}^1 = \boldsymbol{A}^{1/0}.\boldsymbol{e}^0 \quad \text{and.} \quad \overline{\boldsymbol{e}}^2 = \boldsymbol{A}^{2/0}.\boldsymbol{e}^0 \tag{72}$$

with

$$\begin{aligned} \boldsymbol{A}^{1/0} &= \left[\boldsymbol{I} + \boldsymbol{L}_0^{\Omega_2}.\left(\phi_1\,\Delta\boldsymbol{k}^{1/0} + \phi_2\,\Delta\boldsymbol{k}^{2/0}\right) + \phi_2\left(\boldsymbol{I} + \boldsymbol{L}_0^{\Omega_2}.\Delta\boldsymbol{k}^{2/0}\right).\boldsymbol{L}_2^2.\Delta\boldsymbol{k}^{1/2}\right]^{-1} \\ \boldsymbol{A}^{2/0} &= \left(\boldsymbol{I} + \boldsymbol{L}_2^2.\Delta\boldsymbol{k}^{1/2}\right).\boldsymbol{A}^{1/0} \end{aligned} \tag{73}$$

By assuming orthotropic thermal conductivity per phase, localization tensors $\boldsymbol{A}^{1/0}$ and $\boldsymbol{A}^{2/0}$ appear also orthotropic [31] and the i^{th} component, for $i \in \{1,2,3\}$ reads:

$$\begin{aligned} A_i^{1/0} &= \left[1 + L_{0_i}^{\Omega_2}\left(\phi_1\,\Delta {k_i}^{1/0} + \phi_2\,\Delta {k_i}^{2/0}\right) + \phi_2\left(I + L_{0_i}^{\Omega_2}\,\Delta {k_i}^{2/0}\right) L_{2_i}^2\,\Delta {k_i}^{1/2}\right]^{-1} \\ A_i^{2/0} &= \left(1 + L_{2_i}^2 \Delta {k_i}^{1/2}\right) A_i^{1/0}. \end{aligned} \tag{74}$$

The components of tensors $\boldsymbol{L}_2^1$, $\boldsymbol{L}_2^2$, $\boldsymbol{L}_2^{\Omega_2}$ and $\boldsymbol{L}_0^{\Omega_2}$ are deduced from Eq.(52) by putting $\tilde{\lambda}_1 = \tilde{\lambda}_2 = 0$:

$$L_{0_i}^{\Omega_2} = \frac{\tilde{I}_i\left(\tilde{b}_i^0, 0\right)}{4\pi\, k_i^0}; \quad L_{2_i}^1 = \frac{\tilde{I}_i(\tilde{a}_i^2, 0)}{4\,\pi\, k_i^2}; \quad L_{2_i}^{\Omega_2} = \frac{\tilde{I}_i\left(\tilde{b}_i^2, 0\right)}{4\,\pi\, k_i^2} \quad \text{and} \quad \boldsymbol{L}_2^2 = \boldsymbol{L}_2^{\Omega_2} - \frac{\Omega_2}{V_2}\left(\boldsymbol{L}_2^{\Omega_2} - \boldsymbol{L}_2^{\Omega_1}\right) \tag{75}$$

with

$$\tilde{b}_i^0 = \frac{b_i}{\gamma_i^0}, \tilde{a}_i^2 = \frac{a_i}{\gamma_i^2}, \tilde{b}_i^2 = \frac{b_i}{\gamma_i^2}; \quad \gamma_i^* = \sqrt{k_i^*/k_1^*} \quad \text{for} \quad *= 0, 2 \text{ and } i = 1, 2, 3.$$

Transformed ellipsoids $\widetilde{\Omega}_1$ and $\widetilde{\Omega}_2$ are assumed confocal so that (see Appendix B):

$$\left(\tilde{b}_1\right)^2 - (\tilde{a}_1)^2 = \left(\tilde{b}_2\right)^2 - (\tilde{a}_2)^2 = \left(\tilde{b}_3\right)^2 - (\tilde{a}_3)^2$$

In the particular case of isotropic thermal conductivity per phase, Eqs.(74) are the same as results of Stepin [15]. In the particular case of isotropic thermal conductivity of phase *'2'* and HRM ($\boldsymbol{k}^2 = k^2\boldsymbol{I}$, $\boldsymbol{k}^0 = k^0\boldsymbol{I}$), we retrieve the localization relationships obtained by Giordano [17]. Moreover, for anisotropic thermal conductivity per local phase, localization expressions Eqs. (74) coincide with those suggested by Lavrov and Yakovlev [20].

4.2. Doubly coated inclusion ($N = 3$)

We consider an ellipsoidal inclusion with volume V_1 and semi-axis a_1, a_2, a_3, surrounded by an interphase with volume V_2 and the matrix with volume V_3. b_1, b_2 and b_3 (respectively c_1, c_2 and c_3) are the semi-axis of ellipsoidal composite inclusion $\Omega_2 = V_1 + V_2$ (respectively $\Omega_3 = \Omega_2 + V_3$) as depicted by Fig.3. Composite inclusion Ω_3 is assumed embedded in an HRM denoted '*0*'. Let $\boldsymbol{k}^1$, $\boldsymbol{k}^2$, $\boldsymbol{k}^3$ and $\boldsymbol{k}^0$ represent the thermal conductivity respectively of inclusion, interphase, matrix and HRM.

From Eq.(21), the averaged intensity over the composite-inclusion Ω_3 is expressed as:

$$\overline{\boldsymbol{e}}^{\Omega_3} = \boldsymbol{e}^0 - \phi_1 \boldsymbol{L}_0^{\Omega_3}.\Delta\boldsymbol{k}^{1/0}.\overline{\boldsymbol{e}}^1 - \phi_2 \boldsymbol{L}_0^{\Omega_3}.\Delta\boldsymbol{k}^{2/0}.\overline{\boldsymbol{e}}^2 - \phi_3 \boldsymbol{L}_0^{\Omega_3}.\Delta\boldsymbol{k}^{3/0}.\overline{\boldsymbol{e}}^3. \tag{76}$$

where $\boldsymbol{L}_0^{\Omega_3}$ is the interior-point Eshelby's conduction tensor associated to $\boldsymbol{k}^0$ and to ellipsoidal volume Ω_3 defined by Eq.(20). Eq.(59) provides two complementary relations as:

$$\overline{\boldsymbol{e}}^{\Omega_2} = \overline{\boldsymbol{e}}^1 + \frac{\phi_2}{\phi_1 + \phi_2}\boldsymbol{L}_2^{(2)}.\Delta\boldsymbol{k}^{1/2}.\overline{\boldsymbol{e}}^1 \tag{77}$$

$$\overline{\boldsymbol{e}}^{\Omega_3} = \overline{\boldsymbol{e}}^{\Omega_2} + \frac{\phi_3}{\phi_1 + \phi_2}\boldsymbol{L}_3^{(3)}.\left(\phi_1\,\Delta\boldsymbol{k}^{1/3}.\overline{\boldsymbol{e}}^1 + \phi_2\,\Delta\boldsymbol{k}^{2/3}.\overline{\boldsymbol{e}}^2\right). \tag{78}$$

Eshelby's tensors $\boldsymbol{L}_3^{\Omega_3}$ and $\boldsymbol{L}_3^{\Omega_2}$ are defined by Eq.(35). The system of Eqs.(76) to (78) is then solved to express of $\overline{\boldsymbol{e}}^1$, $\overline{\boldsymbol{e}}^2$ and $\overline{\boldsymbol{e}}^3$ as:

$$\overline{\boldsymbol{e}}^P = \boldsymbol{A}^{P/0}.\boldsymbol{e}^0 \quad \text{for} \quad P \in \{1,2,3\}$$

with:

$$\begin{aligned}\boldsymbol{A}^{1/0} = \Bigg[&\phi_1\left(\boldsymbol{I} + \boldsymbol{L}_0^{\Omega_3}.\boldsymbol{\Delta k^{1/0}}\right) + \phi_2\left(\boldsymbol{I} + \boldsymbol{L}_0^{\Omega_3}.\boldsymbol{\Delta k^{2/0}}\right).\left(\boldsymbol{I} + \boldsymbol{L}_2^{(2)}.\Delta\boldsymbol{k}^{1/2}\right)\\ &+ \phi_3\left(\boldsymbol{I} + \boldsymbol{L}_0^{\Omega_3}.\boldsymbol{\Delta k^{3/0}}\right).\left(\frac{\phi_1}{\phi_1 + \phi_2}\left(\boldsymbol{I} + \boldsymbol{L}_3^{(3)}.\Delta\boldsymbol{k}^{1/3}\right)\right.\\ &\left.+ \frac{\phi_2}{\phi_1 + \phi_2}\left(\boldsymbol{I} + \boldsymbol{L}_3^{(3)}.\Delta\boldsymbol{k}^{2/3}\right)\right).\left(\boldsymbol{I} + \boldsymbol{L}_2^{(2)}.\Delta\boldsymbol{k}^{1/2}\right)\Bigg]^{-1}\end{aligned} \tag{79}$$

$$\boldsymbol{A}^{2/0} = \left(\boldsymbol{I} + \boldsymbol{L}_2^{(2)}.\Delta\boldsymbol{k}^{1/2}\right).\boldsymbol{A}^{1/0} \tag{80}$$

and

$$\boldsymbol{A}^{3/0} = \frac{\phi_1}{\phi_1+\phi_2}\left(\boldsymbol{I} + \boldsymbol{L}_3^{(3)}.\Delta\boldsymbol{k}^{1/3}\right) + \frac{\phi_2}{\phi_1+\phi_2}\left(\boldsymbol{I} + \boldsymbol{L}_3^{(3)}.\Delta\boldsymbol{k}^{2/3}\right).\boldsymbol{A}^{2/0}. \tag{81}$$

Transformed ellipsoids $\widetilde{\Omega}_1$, $\widetilde{\Omega}_2$ and $\widetilde{\Omega}_3$ are assumed confocal (see Appendix B):

$\left(\tilde{b}_1\right)^2 - (\tilde{a}_1)^2 = \left(\tilde{b}_2\right)^2 - (\tilde{a}_2)^2 = \left(\tilde{b}_3\right)^2 - (\tilde{a}_3)^2$ and $(\tilde{c}_1)^2 - \left(\tilde{b}_1\right)^2 = (\tilde{c}_2)^2 - \left(\tilde{b}_2\right)^2 = (\tilde{c}_3)^2 - \left(\tilde{b}_3\right)^2$

In the following, we apply the present model to a three-phase composite that consists of inclusions denoted "I" of volume fraction f_I surrounded by a coating denoted "c" of volume fraction f_c, both embedded in the matrix denoted "M". Thermal conductivity of local phases is described by $\boldsymbol{k}^I$, $\boldsymbol{k}^c$ and $\boldsymbol{k}^M$. By putting:

$$\overline{\boldsymbol{e}}^I = \boldsymbol{A}^I.\boldsymbol{E} \quad \text{and} \quad \overline{\boldsymbol{e}}^c = \boldsymbol{A}^c.\boldsymbol{E} \tag{82}$$

Effective thermal conductivity $\boldsymbol{k}^{eff}$ reads:

$$\boldsymbol{k}^{eff} = \boldsymbol{k}^M + f_I\,(\boldsymbol{k}^I - \boldsymbol{k}^M).\boldsymbol{A}^I + f_c\,(\boldsymbol{k}^c - \boldsymbol{k}^M).\boldsymbol{A}^c. \tag{83}$$

Through the GSC scheme, the corresponding three-phase composite inclusion is assumed surrounded by a HEM with thermal conductivity $\boldsymbol{k}^{eff}$. In this case, intensity localization tensors in the inclusion and the coating are obtained by solving the system of Eqs. (60) and (70):

$$\begin{aligned}\boldsymbol{A}^{I/eff} &= \left[\boldsymbol{I} + \frac{1}{f_I+f_c}\left(f_c\,\boldsymbol{L}_c^{\mathrm{c}}.\Delta\boldsymbol{k}^{I/c} + f_M\,\boldsymbol{L}_M^{\mathrm{M}}\left(f_I\,\Delta\boldsymbol{k}^{I/M} + f_c\,\Delta\boldsymbol{k}^{c/M} + f_c\,\Delta\boldsymbol{k}^{c/M}.\boldsymbol{L}_c^{\mathrm{c}}.\Delta\boldsymbol{k}^{I/c}\right)\right)\right]^{-1} \\ \boldsymbol{A}^{c/eff} &= \left(\boldsymbol{I} + \boldsymbol{L}_c^{\mathrm{c}}.\Delta\boldsymbol{k}^{I/c}\right).\boldsymbol{A}^{I/eff}.\end{aligned} \tag{84}$$

For spherical inclusions and isotropic thermal conductivity per phase, obtained expressions of the effective thermal conductivity are the same as those provided by Hervé [17].

5. Effective thermal conductivity of a three-phase composite material

We consider a three-phase composite made of inclusions ($\boldsymbol{k}^I$) surrounded by a coating ($\boldsymbol{k}^c$) and embedded in a matrix with thermal conductivity ($\boldsymbol{k}^M$). Let f_I, f_c and $f_2 = f_I + f_c$ represent the volume fraction of inclusions, coating and the composite inclusion (inclusion+coating), respectively.

Within GMT scheme, the three-phase composite is represented by a simply coated inclusion embedded in the matrix. Thus, from Eq.(73) and by putting $\boldsymbol{k}^0 = \boldsymbol{k}^M$, we obtain:

$$\begin{aligned} \boldsymbol{A}^{I/M} &= \left[\boldsymbol{I} + \boldsymbol{L}_M^{\Omega_2}.\left(\phi_1\,\Delta\boldsymbol{k}^{I/M} + \phi_2\,\Delta\boldsymbol{k}^{c/M}\right) + \phi_2\left(\boldsymbol{I} + \boldsymbol{L}_M^{\Omega_2}.\Delta\boldsymbol{k}^{c/M}\right).\boldsymbol{L}_c^c.\Delta\boldsymbol{k}^{I/c}\right]^{-1} \\ \boldsymbol{A}^{c/M} &= \left(\boldsymbol{I} + \boldsymbol{L}_c^c.\Delta\boldsymbol{k}^{I/c}\right).\boldsymbol{A}^{I/M} \end{aligned} \tag{85}$$

Localization of intensity are then deduced from Eqs.(67):

$$\boldsymbol{A}^M = \left[\boldsymbol{I} + f_1\,\boldsymbol{A}^{I/M} + f_c\,\boldsymbol{A}^{c/M}\right]^{-1},\quad \boldsymbol{A}^I = \boldsymbol{A}^{I/M}.\boldsymbol{A}^M \quad \text{and} \quad \boldsymbol{A}^c = \boldsymbol{A}^{c/M}.\boldsymbol{A}^M \tag{86}$$

5.1. Composite materials with spheroidal inclusions

Inclusions are assumed spheroidal of semi-axis $a_1 \neq a_2 = a_3$ with aspect ratio $\alpha = a_3/a_1$. Aspect ratios β and γ of composite inclusions Ω_2 and Ω_3 are defined by $\beta = b_3/b_1 = b_3/b_2$ and $\gamma = c_3/c_1 = c_3/c_2$ are evaluated by solving equation (B-9) given in Appendix B.

The thermal conductivity of local phases is assumed isotropic. The present section aims to compare the effective thermal conductivity as predicted by both GMT and GSC schemes. For numerical applications, we considered $k^I/k^M = 100$ and $k^c/k^M = 10$. Figs 4a and 4b compare longitudinal and transversal effective thermal conductivity as a function of the volume fraction of inclusions, for $\alpha = 5$.

For GMT scheme, aspect ratio β of the composite inclusion (simply coated inclusion) is deduced as detailed in Appendix B:

$$(\alpha^2 - 1)\left(\frac{f_I}{f_2}\,\frac{\beta}{\alpha}\right)^{\frac{2}{3}} = \beta^2 - 1 \tag{87}$$

Within GSC formulation, a doubly coated inclusion embedded in a HME is considered. In this case, aspect ratios β and γ result from following system of two equations:

$$(\alpha^2-1)\left(f_I\,\frac{\gamma}{\alpha}\right)^{\frac{2}{3}}=(\beta^2-1)\left(f_2\,\frac{\gamma}{\beta}\right)^{\frac{2}{3}},\quad (\beta^2-1)\left(f_2\,\frac{\gamma}{\beta}\right)^{\frac{2}{3}}=(\gamma^2-1) \tag{88}$$

Obtained curves as predicted by both schemes show the same trend. As expected, since $k^I/k^M = 100$, the effective conductivity increases with the volume fraction of inclusions, whatever the ratio f_c/f_I. Up to $f_I = 10\%$, GMT and GSC schemes both predict the similar effective conductivity. But beyond this value of volume fraction of inclusions, the deviations between predictions of both models increase with f_I. Theses deviations are more significant in the longitudinal direction than in transversal one. GSC model predicts higher values of effective thermal conductivity than GMT model.

Comparisons of GMT and GSC predictions have been also performed in terms of the effects of the aspect ratio α of the core (Fig. 5). For the considered prolate spheroid inclusion, the highest component of the effective thermal conductivity is noticed in the direction corresponding to the major semi-axis of the ellipsoidal inclusion. In the longitudinal direction k_{11}^{eff}/k^M increases with the aspect ratio $\alpha = a_1/a_3$. On contrary, in transverse directions, k_{22}^{eff}/k^M or k_{33}^{eff}/k^M decreases with α. As expected, GMT and GSC schemes predict the same value for spherical inclusions. For non-spherical inclusions, as previously some deviations between GMT and GSC predictions are observed for both components of the effective conductivity. Effective properties as predicted by GSC remain superior to those issued from GMT model. It should be noted that the relevance of GMT predictions is limited to materials with small volume fractions of inclusions.

5.2. Comparison with Finite Elements Methods

For a three-phase composite material, the effective conductivity as predicted by the present model through a '3+1-phase' model is compared with some numerical provided by finite elements methods (FEM) due to Ahmadi et *al*. [32]. Fig.6 depicts the effective thermal conductivity of a

three-phase material that consists of uniaxially oriented coated carbon fiber embedded in cement matrix. As in [32], the isotropic thermal conductivities of the fiber, interphase and cement matrix are taken as $k^I = 222\ W.m^{-1}.K^{-1}$, $k^c = 5.3\ W.m^{-1}.K^{-1}$ and $k^M = 0.53\ W.m^{-1}.K^{-1}$, respectively. The carbon fiber diameter is taken as $10\ \mu m$ and the interphase thickness is equal to $1\ \mu m$.

Fig.6a shows that the longitudinal ETC linearly increases with the fiber volume fraction. Indeed, for this case of uniaxially oriented fibers, the longitudinal ETC is mainly dominated by fiber conductivity. In Fig.6b, transverse ETC also increases with fiber volume fraction. The slop is at first soft up to 30% of fiber volume fraction and gets steeper and steeper beyond this value.

For both longitudinal and transverse ETC, the present model and FEM [32] predict similar results, whatever the fiber volume fraction.

The present model's predictions were also compared with interphase model with the FE homogenization method proposed by Tian et *al*. [33]. The considered RVE consists of aligned ellipsoidal inclusions, each surrounded by an interphase, both embedded in a matrix. The inclusion major length is $20\ \mu m$, the inclusion minor length $10\ \mu m$, the interphase thickness $50\ nm$. Fig.7 presents the longitudinal and transverse ETCs of the composites with the weakly conducting (WC) and highly conducting (HC) interfaces, as predicted by using the interphase model with the FE homogenization method [33] and results of present model. For ellipsoidal inclusions with a volume fraction $f = 0.3$, the thermal conductivity of inclusions is transversely isotropic: $k_I^L = 393\ W.m^{-1}.K^{-1}$, $k_I^T = 50\ W.m^{-1}.K^{-1}$ while the thermal conductivities of the matrix and interphase are isotropic: $k_M = 173\ W.m^{-1}.K^{-1}$. For an WC interphase $k_c = 5\ W.m^{-1}.K^{-1}$ (Figs.7a and 7b) and $k_M = 2 \times 10^4\ W.m^{-1}.K^{-1}$ for HC interphase. Although some small deviations, the FEM [33] predicts similar results as the present model. These deviations are coherent with those as initially pointed out in [33], by comparing FEM predictions with some micromechanical models of imperfect interfaces.

5.3. *Analysis of some model's parameters*

This section aims to analysis the effects of some parameters such as the thermal conductivity of the interphase and its anisotropy on the predicted effective thermal conductivity.

5.3.1. *Influence of the thermal conductivity of the coating*

By assuming isotropic thermal conductivity per local phase, we have also analyzed the effect of the ratio k^c/k^M on the normalized effective conductivity components k_{11}^{eff}/k^M and k_{33}^{eff}/k^M for three selected values of aspect ratio α of a prolate spheroidal inclusion. Corresponding results, as predicted by GSC model for a three-phase composite material are depicted in Figs.8a and 8b.

As Benveniste [34], we noticed two steps in the sigmoid curves : limiting values are obtained for weakly and highly conducting interphase, the plateau enclosed between these limits corresponds to peculiar contrast k^c/k^M that depends on the aspect ratio α.

In the longitudinal direction, when $k^c/k^M \ll 1$, the effect of the aspect ratio k^c/k^M of the inclusion on k_{11}^{eff}/k^M is hardly noticeable. On contrary, as stated previously for $k^c/k^M \gg 1$, the effective conductivity k_{11}^{eff}/k^M increases with the aspect ratio α, from the spherical to the spheroidal shape.

In the transverse direction, $k_{33}^{eff}/k^M = k_{22}^{eff}/k^M$, whatever k^c/k^M the effective conductivity decreases with the aspect ratio α.

5.3.2. *Anisotropy of thermal conductivity of the coating*

Since the developed approach is able to deal with anisotropic thermal conductivity per phase, in the following we analyze the effect the anisotropy of the thermal conductivity of the coating phase on the effective conductivity. For this purpose, we considered transverse isotropic behavior for the coating defined by $k_{11}^c = \eta\, k_{22}^c = \eta\, k_{33}^c$. Aspect ratios β and γ of composite inclusions Ω_2 and Ω_3 are evaluated from equations (B-9) in Appendix B with $f_I = 0.3$, $f_c = 0.1 f_I$ and $\alpha = 5$, as function

of the anisotropic coefficient η. Fig.9 depicts the longitudinal effective thermal conductivity as a function of the ratio k_{33}^{c}/k^{M} for three values of η.

We retrieve the typical sigmoid curves (Fig. 9) observed by Benveniste [34]. The anisotropy of the thermal behavior of the coating induces a shift of the plateau enclosing the limits of the effective conductivities obtained for weakly and highly conducting interphase. The plateau breadth decreases when the conductivity in the principal axes of the prolate increases. This phenomenon is coherent with the better heat transfer induced by higher conductivity.

5.4. Composite materials with ellipsoidal mutli-coated inclusions

The proposed model deals with arbitrary ellipsoidal morphology of multi-coated inclusions. In the present section, we analyze the predictions of the developed model for a three-phase composite material with ellipsoidal inclusions. Inclusions, composite inclusions Ω_2 and Ω_3 have therefore ellipsoidal shapes. Let $(\alpha_1 = a_1/a_3,\ \alpha_2 = a_2/a_3)$, $(\beta_1 = b_1/b_3,\ \beta_2 = b_2/b_3\ )$ and $(\gamma_1 = c_1/c_3,\ \gamma_2 = c_2/c_3)$ denote aspect ratios respectively of inclusion, Ω_2 and Ω_3. By assuming isotropic thermal conductivity per local phase, confocally conditions lead to:

$$(\alpha_1{}^2 - 1)\left(f_I\ \frac{\gamma_1\,\gamma_2}{\alpha_1\,\alpha_2}\right)^{\frac{2}{3}} = (\beta_1{}^2 - 1)\left(f_2\,\frac{\gamma_1\,\gamma_2}{\beta_1\,\beta_2}\right)^{\frac{2}{3}},$$

$$(\alpha_2{}^2 - 1)\left(f_I\ \frac{\gamma_1\,\gamma_2}{\alpha_1\,\alpha_2}\right)^{\frac{2}{3}} = (\beta_2{}^2 - 1)\left(f_2\ \frac{\gamma_1\,\gamma_2}{\beta_1\,\beta_2}\right)^{\frac{2}{3}}, \tag{89}$$

$$(\beta_1{}^2 - 1)\left(f_2\ \frac{\gamma_1\,\gamma_2}{\beta_1\,\beta_2}\right)^{\frac{2}{3}} = (\gamma_1{}^2 - 1), \qquad (\beta_2{}^2 - 1)\left(f_2\ \frac{\gamma_1\,\gamma_2}{\beta_1\,\beta_2}\right)^{\frac{2}{3}} = (\gamma_2{}^2 - 1)$$

By defining aspect ratios $(\alpha_1,\ \alpha_2)$, of inclusions, relations of Eq.(89) provide those of ellipsoids Ω_2 and Ω_3. For numerical results, we consider: $\alpha_1 = 5,\ \alpha_2 = 3,\ k^I/k^M = 100,\ k^c/k^M = 10,\ f_c = 0.3$ and $f_c = 0.1\ f_I$. Fig.10 presents the evolution of the three components of the effective thermal conductivity as a function of k^c/k^M, as predicted by a (3+1)-phase GSC model.

The effective thermal conductivity is anisotropic, mainly due to the ellipsoidal morphology of inclusions and composite inclusions. The highest value of effective thermal conductivity is noticed in the direction parallel to the major semi-axis of ellipsoids, whatever the thermal contrast k^c/k^M is.

6. Conclusions

The exact solution of the problem of multi-coated inclusion is obtained within the framework of heat transfer phenomena in the general case of anisotropic conductivity per phase and ellipsoidal inclusions.

The approach is based on the Green's function technique and leads to integral equations of the problem of heterogeneous material. Moreover, concepts of interior- and exterior-point Eshelby's conduction tensors are introduced to express analytically average intensity in each phase of the composite material. Effective conductivity tensors are explicitly obtained through a Generalized Self-Consistent and Mori-Tanaka schemes sustaining anisotropic behavior and coated confocal ellipsoidal inclusions. When the thermal conductivity of each local phase is assumed isotropic, obtained expressions of local intensities and effective thermal conductivity are the same as exact results for simply or doubly coated inclusions (sphere, cylinder and ellipsoid). Moreover, for anisotropic thermal conductivity per phase and simply coated inclusions, local intensities as predicted by the present model agree with those provided by Lavrov and Yakovlev [20]. Furthermore, the predicted effective thermal conductivity is in accordance with results provided by finite elements methods, even for high volume fractions of inclusions and high contrast of thermal behavior between local phases. Strong influences of the aspect ratio of inclusions and interphase parameters (volume fraction, thermal conductivity) on the model predictions are pointed out.

Effects of weakly and highly conducting interphases on the effective thermal conductivity of the composite are also analyzed. Furthermore, obtained results bring out the significant impact of the anisotropy of the thermal conductivity of the interphase on the thermal transfer between phases of the composite.

The present model may be applied to some transfer phenomena such as magnetic permeability, electrical conductivity, dielectric permittivity and diffusion.

Appendix A: *Properties of projection operators Π*

The projection operator $\boldsymbol{\Pi}$ is related to $\boldsymbol{\Gamma}$ by:

$$\boldsymbol{\Pi} = \boldsymbol{\Gamma}.\boldsymbol{k} \tag{A-1}$$

where $\boldsymbol{\Gamma}$ is the modified Green's tensor associated to the thermal conductivity $\boldsymbol{k}$. Operator $\boldsymbol{\Pi}$ is endowed with the following properties :

$$div\boldsymbol{q} = 0 \Leftrightarrow \boldsymbol{\Pi} * \boldsymbol{h}.\boldsymbol{q} = 0 \text{ with } \boldsymbol{h} = \boldsymbol{k}^{-1}. \tag{A-2}$$

$$\boldsymbol{e} = -\boldsymbol{\nabla} T \text{ and } T = -\boldsymbol{e}^0.\boldsymbol{r} \text{ on } \partial V \Leftrightarrow \boldsymbol{\Pi} * \boldsymbol{e} = \boldsymbol{e} - \boldsymbol{e}^0. \tag{A-3}$$

We propose to demonstrate properties (A-2) and (A-3) in the Fourier space.

The Fourier transform $\tilde{G}(\boldsymbol{\omega})$ of the Green's function $G(\boldsymbol{r})$ is defined by:

$$\tilde{G}(\boldsymbol{\omega}) = \int_V G(\boldsymbol{r}) e^{-i\,\boldsymbol{\omega}.\boldsymbol{r}}\, dV \quad \text{and} \quad G(\boldsymbol{r}) = \frac{1}{8\pi^3}\int_{V_\omega} G(\boldsymbol{r}) e^{i\,\boldsymbol{\omega}.\boldsymbol{r}}\, dV_\omega \tag{A.4}$$

where $i^2 = -1$. Following relations hold true:

$\tilde{G}_{,m}(\boldsymbol{\omega}) = -i\,\omega_m\,\tilde{G}(\boldsymbol{\omega})$ and $\tilde{G}_{,mn}(\boldsymbol{\omega}) = -\omega_m\,\omega_n\,\tilde{G}(\boldsymbol{\omega})$.

In the Fourier space, (A-2) becomes:

$$\tilde{q}_p\,\omega_p = 0 \;\Leftrightarrow\; \tilde{\Pi}_{pj} h_{jm} \tilde{q}_m = 0 \tag{A.5}$$

- $\tilde{\Pi}_{pj} = \tilde{\Gamma}_{pl}\,k_{lj} = \tilde{G}\,\omega_p\,\omega_l\,k_{lj}$

  $\tilde{q}_p\,\omega_p = 0 \Longrightarrow \tilde{\Pi}_{pj}\,h_{jm}\,\tilde{q}_m = \tilde{G}\,\omega_p\,\omega_n\,k_{nj}\,h_{jm}\,\tilde{q}_m = \tilde{G}\,\omega_p\,\omega_n\,\tilde{q}_n = 0$

- $\tilde{\Pi}_{pj}\,h_{jm}\,\tilde{q}_m = 0 \Longrightarrow \tilde{G}\omega_p\,\omega_n\,\tilde{q}_n = 0 \Longrightarrow \omega_n\,\tilde{q}_n = 0$

As a consequence, $div\boldsymbol{q} = 0 \Leftrightarrow \boldsymbol{\Pi} * \boldsymbol{h}.\boldsymbol{q} = 0$

Eq.(A-3) becomes in the Fourier space:

$$\tilde{e}_m = i\,\omega_m\,\tilde{T} \text{ and } \tilde{e}_m{}^0 = i\,\omega_m\,\tilde{T}^0 \quad \Leftrightarrow \tilde{\Pi}_{mn}\,\tilde{e}_n = \tilde{e}_m - \tilde{e}_m{}^0 \tag{A.6}$$

- $\tilde{e}_m = i\,\omega_m\,\tilde{T}$ and $\tilde{e}_m{}^0 = i\,\omega_m\,\tilde{T}^0 \;\Longrightarrow\; \tilde{e}_m - \tilde{e}_m{}^0 = \tilde{G}\,k_{pj}\,\omega_p\,\omega_j\left(\tilde{e}_m - \tilde{e}_m{}^0\right) =$

  $\tilde{G}\,k_{pj}\,\omega_p\,\omega_j(i\,\omega_m)\left(\tilde{T} - \tilde{T}^0\right) = \tilde{G}\,\omega_m\,\omega_j\,k_{pj}\left(i\,\omega_p\right)\left(\tilde{T} - \tilde{T}^0\right) = \tilde{\Gamma}_{mj}\,k_{jp}\left(i\,\omega_p\right)\left(\tilde{T} - \tilde{T}^0\right)$

  $= \tilde{\Pi}_{mp}\left(\tilde{e}_p - \tilde{e}_p{}^0\right)$

- $\widetilde{\Pi}_{mj}\,\tilde{e}_j{}^0 = 0 \Longrightarrow \widetilde{\Pi}_{mj}\,\tilde{e}_j = \widetilde{\Pi}_{mj}\big(\tilde{e}_j - \tilde{e}_j{}^0\big) = \tilde{G}\,\omega_m\,\omega_p\,k_{pj}\,\big(i\,\omega_j\big)\big(\tilde{T} - \tilde{T}^0\big) =$

  $\tilde{G}\,k_{pj}\,\omega_m\,\omega_p\big(i\,\omega_j\big)\big(\tilde{T} - \tilde{T}^0\big) = i\,\omega_m\big(\tilde{T} - \tilde{T}^0\big) = \tilde{e}_m - \tilde{e}_m{}^0$

As a consequence, $\boldsymbol{e} = -\boldsymbol{\nabla}T$ and $T = -\boldsymbol{e}^0.\boldsymbol{r}$ on $\partial V \Leftrightarrow \boldsymbol{\Pi} * \boldsymbol{e} = \boldsymbol{e} - \boldsymbol{e}^0$.

Appendix B: *Confocal conditions for the coated ellipsoidal inclusions*

The methodology developed hereafter aims to determine the aspect ratio of the transformed composite inclusion $\widetilde{\Omega}_{\mathrm{P}}$ as function of the inclusion morphology V_1 and the volume fractions f_P of the phase 'P' with thermal conductivity $\boldsymbol{k}^P$:

$$f_P = \frac{V_P}{\Omega_N} \quad \text{and} \quad \Omega_P = \sum_{i=1}^{P} V_i \quad \text{for.}\ P \in \{1, \dots, N\}. \tag{B-1}$$

The volume of ellipsoidal composite inclusion Ω_P is expressed as function of its semi-axes (a_1^P, a_2^P, a_3^P) as:

$$\Omega_P = \frac{4\pi}{3} a_1^P\,a_2^P\,a_3^P \tag{B-2}$$

Consequently, the volume of the transformed ellipsoidal composite inclusions $\widetilde{\Omega}_P$ reads:

$$\widetilde{\Omega}_P = \frac{4\pi}{3} \tilde{a}_1^P\,\tilde{a}_2^P\,\tilde{a}_3^P \tag{B-2}$$

Let us define the aspect ratios β_1^P and β_2^P as:

$$\beta_1^P = \frac{\tilde{a}_3^P}{\tilde{a}_1^P} \quad \text{and} \quad \beta_2^P = \frac{\tilde{a}_3^P}{\tilde{a}_2^P} \quad \text{for} \quad P \in \{1, \dots, N\}. \tag{B-3}$$

The confocally conditions between the composite inclusions $\widetilde{\Omega}_{P-1}$ and $\widetilde{\Omega}_P$ are formulated as:

$$\begin{aligned} (\tilde{a}_{3P}^P)^2 - (\tilde{a}_{1P}^P)^2 &= (\tilde{a}_{3P}^{P-1})^2 - (\tilde{a}_{1P}^{P-1})^2 \\ (\tilde{a}_{3P}^P)^2 - (\tilde{a}_{2P}^P)^2 &= (\tilde{a}_{3P}^{P-1})^2 - (\tilde{a}_{2P}^{P-1})^2 \end{aligned} \tag{B-4}$$

with $\tilde{a}_{iP}^P = \frac{a_i^P}{\gamma_i^P}$ and $\gamma_i^P = \sqrt{\frac{k_i^P}{k_1^P}}$.

By replacing Eqs. (B.2) and (B.3) in (B.1), the following relationships may be written:

$$\frac{\Omega_{P-1}}{\Omega_P} = \frac{\sum_{i=1}^{P-1} f_i}{\sum_{i=1}^{P} f_i} = \left(\frac{\beta_1^{P-1}}{\beta_1^P}\right)^2 \frac{\beta_2^P}{\beta_2^{P-1}} \left(\frac{a_1^{P-1}}{a_1^P}\right)^3 \tag{B-5}$$

The confocally condition Eq. (B-4) between Ω_{P-1} and Ω_P becomes:

$$\left(\frac{\tilde{a}_{1P}^{P-1}}{\tilde{a}_{1P}^{P}}\right)^2 = \frac{\left(\frac{\tilde{a}_{3P}^{P}}{\tilde{a}_{1P}^{P}}\right)^2 - 1}{\left(\frac{\tilde{a}_{3P}^{P-1}}{\tilde{a}_{1P}^{P-1}}\right)^2 - 1} \quad \text{and} \quad \left(\frac{\tilde{a}_{2P}^{P-1}}{\tilde{a}_{2P}^{P}}\right)^2 = \frac{\left(\frac{\tilde{a}_{3P}^{P}}{\tilde{a}_{2P}^{P}}\right)^2 - 1}{\left(\frac{\tilde{a}_{3P}^{P-1}}{\tilde{a}_{2P}^{P-1}}\right)^2 - 1} \tag{B-6}$$

By replacing Eq. (B.6) into Eq. (B.5), the volume fractions f_P for for $P \in \{1, \dots, N\}$ satisfy the following system of non-linear equations:

$$\begin{aligned} \frac{\sum_{i=1}^{P-1} f_i}{\sum_{i=1}^{P} f_i} &= \left(\frac{\beta_1^{P-1}}{\beta_1^P}\right)^2 \frac{\beta_2^P}{\beta_2^{P-1}} \left(\frac{\left(\frac{\tilde{a}_{3P}^{P}}{\tilde{a}_{1P}^{P}}\right)^2 - 1}{\left(\frac{\tilde{a}_{3P}^{P-1}}{\tilde{a}_{1P}^{P-1}}\right)^2 - 1} \right)^{3/2} \\ \frac{\sum_{i=1}^{P-1} f_i}{\sum_{i=1}^{P} f_i} &= \left(\frac{\beta_2^{P-1}}{\beta_2^P}\right)^2 \frac{\beta_1^P}{\beta_1^{P-1}} \left(\frac{\left(\frac{\tilde{a}_{3P}^{P}}{\tilde{a}_{2P}^{P}}\right)^2 - 1}{\left(\frac{\tilde{a}_{3P}^{P-1}}{\tilde{a}_{2P}^{P-1}}\right)^2 - 1} \right)^{3/2} \end{aligned} \tag{B-7}$$

The aspect ratio of the composite inclusion Ω_{P-1} and the thermal behavior of the phase *'P'* provide the parameters $\beta_1^{P-1}, \beta_2^{P-1}$. From the volume fractions f_P, one can express the aspect ratios β_1^P and β_2^P for $P \in \{1, \dots, N\}$ as function of the ratio $\sum_{i=1}^{P-1} f_i \,/\, \sum_{i=1}^{P} f_i$.

- In the case of a simply coated spheroidal inclusion (V_1, Ω_2) defined by semi-axes $(a_1 = a_2 \neq a_3,\ b_1 = b_2 \neq b_3)$, aspect ratios are defined as $\alpha = a_3/a_1 = a_3/a_2$ and $\beta = b_3/b_1 = b_3/b_2$. α and β can be linked to the volume fraction f_1 of inclusion through the following non-linear equation:

$$\tilde{\beta}^6 - 3\,\tilde{\beta}^4 + \left(3 + \frac{(1-\tilde{\alpha}^2)^3}{\tilde{\alpha}^4} {f_1}^2\right)\tilde{\beta}^2 - 1 = 0 \quad \text{with} \quad \tilde{\alpha} = \eta\alpha \quad \text{and} \quad \tilde{\beta} = \eta\beta. \tag{B-8}$$

where $\eta = k_3^2/k_1^2 = k_3^2/k_2^2$.

- In the case of a doubly coated spheroidal inclusion $(V_1, \Omega_2, \Omega_3)$ defined by their semi-axes $(a_1 = a_2 \neq a_3,\ b_1 = b_2 \neq b_3,\ c_1 = c_2 \neq c_3)$, aspect ratios are defined as $\alpha = a_3/a_1 = a_3/a_2$,$\beta = b_3/b_1 = b_3/b_2$ and $\gamma = c_3/c_1 = c_3/c_2$. Aspect ratios α, β and γ are related to volume fractions $f_{1c} = f_1/(f_1 + f_c)$ and $f_{cM} = f_1 + f_c = \gamma\, b_1^3/\beta\, c_1^3$ through following non-linear equations :

$$\tilde{\beta}_2^6 - 3\,\tilde{\beta}_2^4 + \left(3 + \frac{(1-\tilde{\alpha}^2)^3}{\tilde{\alpha}^4} {f_{1c}}^2\right)\tilde{\beta}_2^2 - 1 = 0 \quad \text{with} \quad \tilde{\alpha} = \eta_2\alpha. \text{ and } \tilde{\beta}_2 = \eta_2\beta$$

$$\tilde{\gamma}^6 - 3\,\tilde{\gamma}^4 + \left(3 + \frac{\left(1-\tilde{\beta}_3^2\right)^3}{\tilde{\beta}_3^4} {f_{cM}}^2\right)\tilde{\gamma}^2 - 1 = 0 \quad \text{with} \quad \tilde{\gamma} = \eta_3\gamma \quad \text{and} \quad \tilde{\beta}_3 = \eta_3\beta \tag{B-9}$$

$\eta_2 = k_3^2/k_1^2 = k_3^2/k_2^2$ and $\eta_3 = k_3^3/k_1^3 = k_3^3/k_2^3$.

References

[1] L. Wang, J. Li, M. Catalano, G. Bai, N. Li, J. Dai, X. Wang, H. Zhang, J. Wang, M.J. Kim, Enhanced thermal conductivity in Cu / diamond composites by tailoring the thickness of interfacial TiC layer, Compos. Part A. 113 (2018) 76–82. doi:10.1016/j.compositesa.2018.07.023.

[2] L. Wang, J. Li, Z. Che, X. Wang, H. Zhang, J. Wang, M.J. Kim, Combining Cr pre-coating and Cr alloying to improve the thermal conductivity of diamond particles reinforced Cu matrix composites, J. Alloys Compd. 749 (2018) 1098–1105. doi:10.1016/j.jallcom.2018.03.241.

[3] R. Pei, G. Chen, Y. Wang, M. Zhao, G. Wu, Effect of interfacial microstructure on the thermal-mechanical properties of mesophase pitch-based carbon fiber reinforced aluminum composites, J. Alloys Compd. 756 (2018) 8–18. doi:10.1016/j.jallcom.2018.04.330.

[4] J.D. Eshelby, The determination of the elastic field of an ellipsoidal inclusion, and related problems, Proc. R. Soc. London, A. 241 (1957) 376–396.

[5] B.A. Aboudi, J., Arnold, S. M., & Bednarcyk, Micromechanics of composite materials: a generalized multiscale analysis approach, 2012.

[6] R.M. Christensen, Viscoelastic properties of heterogeneous media, J. Mech. Phys. Solids. 17 (1969) 23–41.

[7] R.M. Christensen, K.H. Lo, Solutions for effective shear properties in three phase sphere and cylinder models, J. Mech. Phys. Solids. 27 (1979) 315–330.

[8] J.C. Maxwell, A Treatise on Electricity and Magnetism, vol1, Clarendon , Oxford, 1873.

[9] L. Rayleigh, On the influence of obstacles arranged in rectangular order upon the properties of the medium, Philosophical Magazine 1892; 34: 481-502.

[10] Z. Hashin, S. Shtrikman S, A variational approach to the theory of the effective magnetic permeability of multiphase materials. Journal of Applied Physics 33 (1962) 3125–3131.

[11] Z. Hashin, Assessment of the self consistent approximation : conductivity of particulate composites, J. Compos. Mater. 2 (1968) 284–300.

[12] E. Herve, Thermal and thermoelastic behaviour of multiply coated inclusion-reinforced composites, Int. J. Solids Struct. 39 (2002) 1041–1058.

[13] R.-B. Yang, Y.-M. Lee, Y.C. Shiah, T.-W. Tsai, On the generalized self-consistent model for the effective conductivity of composites reinforced by multi-layered orthotropic fibers, Int. Communications. Heat Mass Transf. 49 (2013) 55–59.

[14] O.D. Kellogg, Foundations of Potential Theory. Berlin Heidelberg London. Springer-Verlag. 1953.

[15] L.D. Stepin, Dielectric permeability of a medium with nonuniform ellipsoidal inclusions, Sov. Phys. Tech. Physics-USSR. 10 (1965) 768.

[16] H. Hatta , M. Taya, Thermal conductivity of coated filler composites, J. Appl. Phys. 59 (1986) 1851–1860. doi:10.1063/1.336412.

[17] S. Giordano, Nonlinear effective behavior of a dispersion of randomly oriented coated ellipsoids with arbitrary temporal dispersion, Int. J. Eng. Sci. 33 (2015) 1–22.

[18] Y. Benveniste, T. Chen, G.J. Dvorak, The effective thermal conductivity of composites reinforced by coated cylindrically orthotropic fibers, J. Appl. Phys. 2878 (1990) 2878–2884. doi:10.1063/1.345463.

[19] V.I. Kolesnikov, V.V. Bardushkin, I.V. Lavrov, A.P. Sychev, V. B. Yakovlev, A Generalized effective-field approximation for an Inhomogeneous medium with coated inclusions, Doklady Physics. 476 (2017) 280–284.

[20] I.V. Lavrov, V. B. Yakovlev, Ellipsoidal inclusion with a shell in an anisotropic medium subjected to a uniform electric field, Theoretical and Mathematical Phys. 88 (2018) 1482–1491.

[21] M. Hori, S. Nemat-Nasser, Double-inclusion model and overall moduli of multi-phase

composites, Mech. Mater. 14 (1993) 189–206.

[22] J. Yu, T.E. Lacy, H. Toghiani, C.U. Pittman, Micromechanically-based effective thermal conductivity estimates for polymer nanocomposites, Compos. Part B. 53(2013) 267-273.

[23] S.Y. Kim, Y.J. Noh, J. Yu, Prediction and experimental validation of electrical percolation by applying a modified micromechanics model considering multiple heterogeneous inclusions, Compos. Sci. Technol. 106 (2015) 156–162. doi:10.1016/j.compscitech.2014.11.015.

[24] I.A. Kunin, Elastic Media with Microstructure II: Three Dimensionnal Models, in: Springer S, Berlin, Heidelberg, New-York, Tokyo, 1983.

[25] A. Aboutajeddine, K. W. Neale, The double-inclusion model: A new formulation and new estimates, Mech. of Mater. 37 (2005) 331–341. doi:10.1016/j.mechmat.2003.08.016.

[26] F. Dinzart, H. Sabar, S. Berbenni, Homogenization of multi-phase composites based on a revisited formulation of the multi-coated inclusion problem, Int. J. Eng. Sci. 100 (2016) 136–151.

[27] F. Dinzart, A. Jeancolas, N. Bonfoh, H. Sabar, M. Mihaluta, Micromechanical modeling of the multi- coated ellipsoidal inclusion: application to effective thermal conductivity of composite materials, Arch. Appl. Mech. 88 (2018) 1929–1944. doi: 10.1007/s00419-018-1418-2.

[28] S. Giordano, P.L. Palla, Dielectric behavior of anisotropic inhomogeneities : interior and exterior point Eshelby tensors, J. Phys. A Math. Theor. 41 (2008).

[29] T. Mura, Micromechanics of defects in Solids, Kluwer Academic Publisher, Boston, 1987.

[30] Mori T, Tanaka K. Average stress in matrix and average elastic energy of materials with misfitting inclusions. Acta Metallurgica. 21 (1973) 571-574.

[31] N. Bonfoh, C. Dreistadt, H. Sabar, Micromechanical modeling of the anisotropic thermal conductivity of ellipsoidal inclusion-reinforced composite materials with weakly conducting

interfaces, Int. J. Heat Mass Transf. 108 (2017) 1727–1739. doi:10.1016/j.ijheatmasstransfer.2016.12.008.

[32] M. Ahmadi, R. Ansari, M. Kazem Hassanzadeh-Aghdam, Finite element analysis of thermal conductivities of unidirectional multiphase composites, Composite Interfaces Vol. 26, No. 12 (2019), 1035–1055 https://doi.org/10.1080/09276440.2019.1578588.

[33]. W. Tian, M.W. Fu, L. Qi, X. Chao, J. Liang, Interphase model for FE prediction of the effective thermal conductivity of the composites with imperfect interfaces, Int. J. of Heat and Mass Transfer 145 (2019) 118796.

[34] Y. Benveniste, Models of thin interphases and the effective medium approximation in composite media with curvilinearly anisotropic coated inclusions, Int. J. Eng. Sci. 72 (2013) 140–154. doi:10.1016/j.ijengsci.2013.07.003.

Figure captions

Fig. 1 Topology of the multi-coated inclusion.

Fig. 2 Topology of the simply coated inclusion.

Fig. 3 Topology of the doubly coated inclusion.

Fig.4 Normalized effective conductivity versus volume fraction of prolate inclusions as predicted by GSC and GMT schemes as a function of inclusions' volume fraction: $\alpha = 5$, $k^I/k^M = 100$, $k^c/k^M = 10$; *a-longitudinal direction* (k_{11}^{eff}/k^M), *b-transverse direction* (k_{33}^{eff}/k^M)

Fig. 5 Normalized effective conductivity versus volume fraction of prolate inclusions as predicted by GSC and GMT schemes as a function of inclusions' aspect ratio α: $k^I/k^M = 100$, $k^c/k^M = 10$, $f_I = 0.3$ and $f_c = 0.1\ f_I$.

Fig. 6 Effective thermal conductivity (ETC) versus volume fractions of inclusions: (a) longitudinal ETC and (b) transverse ETC

Fig. 7 Effective thermal conductivity (ETC) versus interphase's thermal conductivity: (a) and (b) longitudinal and transverse ETCs of WC interphase; (c) and (d) longitudinal and transverse ETCs of WC interphase.

Fig. 8: Normalized effective conductivity (GSC scheme) as a function of ratio k^1/k^M for 3 aspect ratios α of prolate inclusions: $k^I/k^M = 100$, $f_I = 0.3$ and $f_c = 0.1\ f_I$.

Fig. 9: Normalized effective conductivity k_{11}^{eff}/k^M as a function of contrast ratio k_{33}^c/k^M for prolate spheroidal inclusion: effect of anisotropy of thermal conductivity of interphase k_{11}^c/k_{33}^c: $\alpha = 5$, $f_I = 0.3$, $f_c = 0.1\ f_I$ and $k^I/k^M = 10$

Fig. 10: Components of normalized effective conductivity as function of ratio k^c/k^M for an ellipsoidal inclusion with aspects ratios $\alpha_1 = 5$, $\alpha_2 = 3$, $k^I/k^M = 100$, $f_I = 0.3$ and $f_c = 0.1\ f_I$.

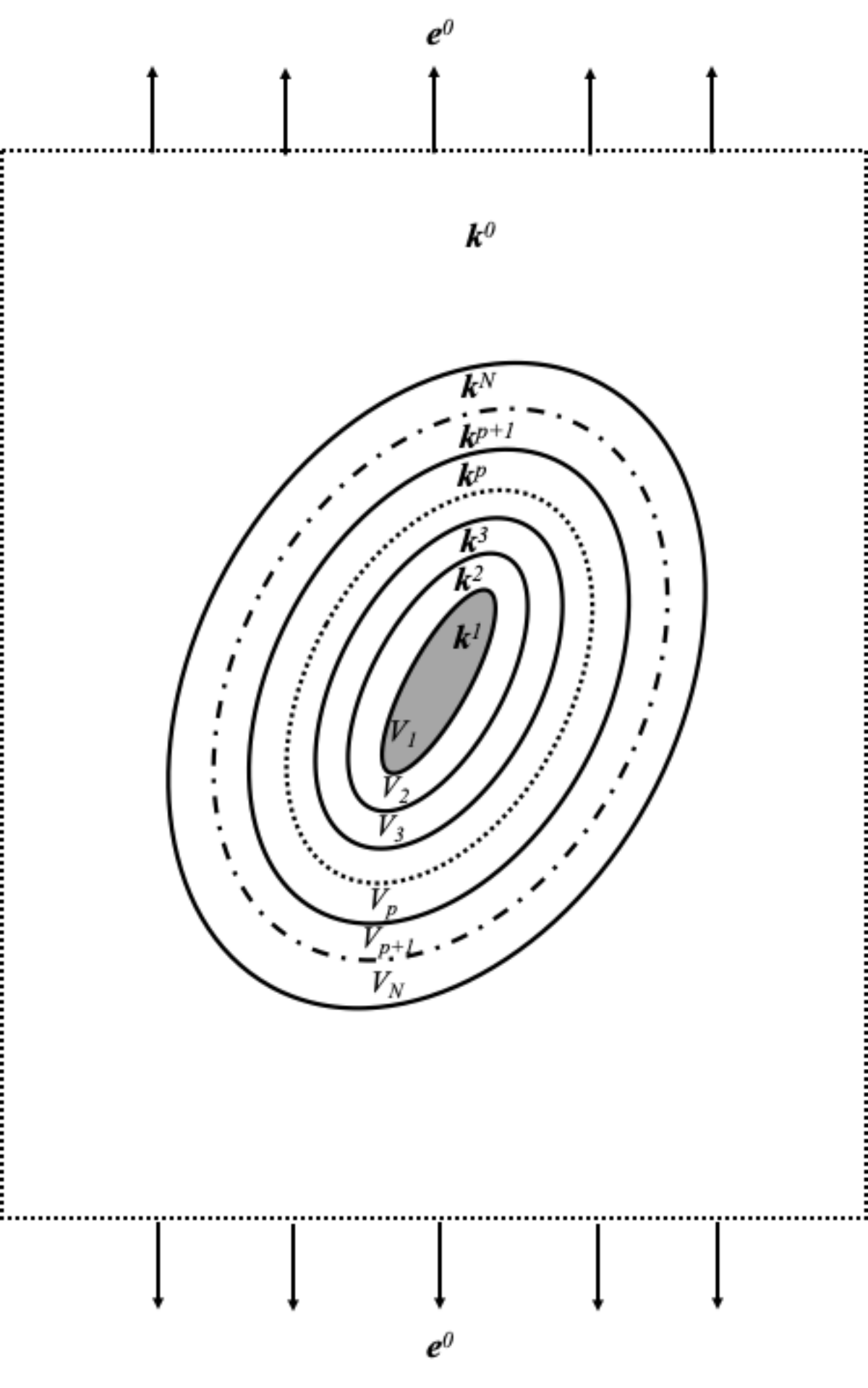
e^0
k^0
k^N
k^{p+1}
k^p
k^3
k^2
k^1
V_1
V_2
V_3
V_p
V_{p+1}
V_N
e^0

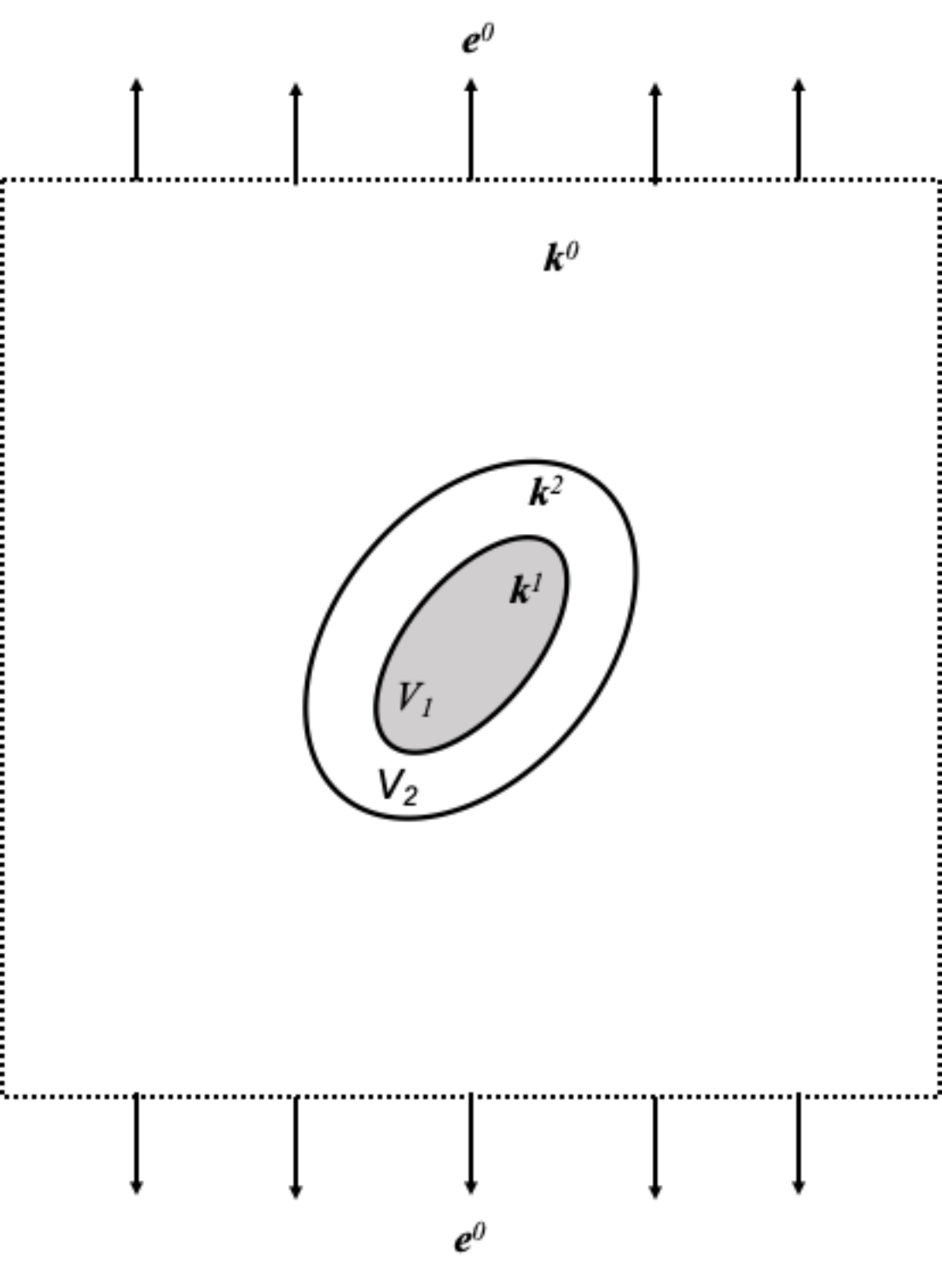
e0
k0
k2
k1
V1
V2
e0

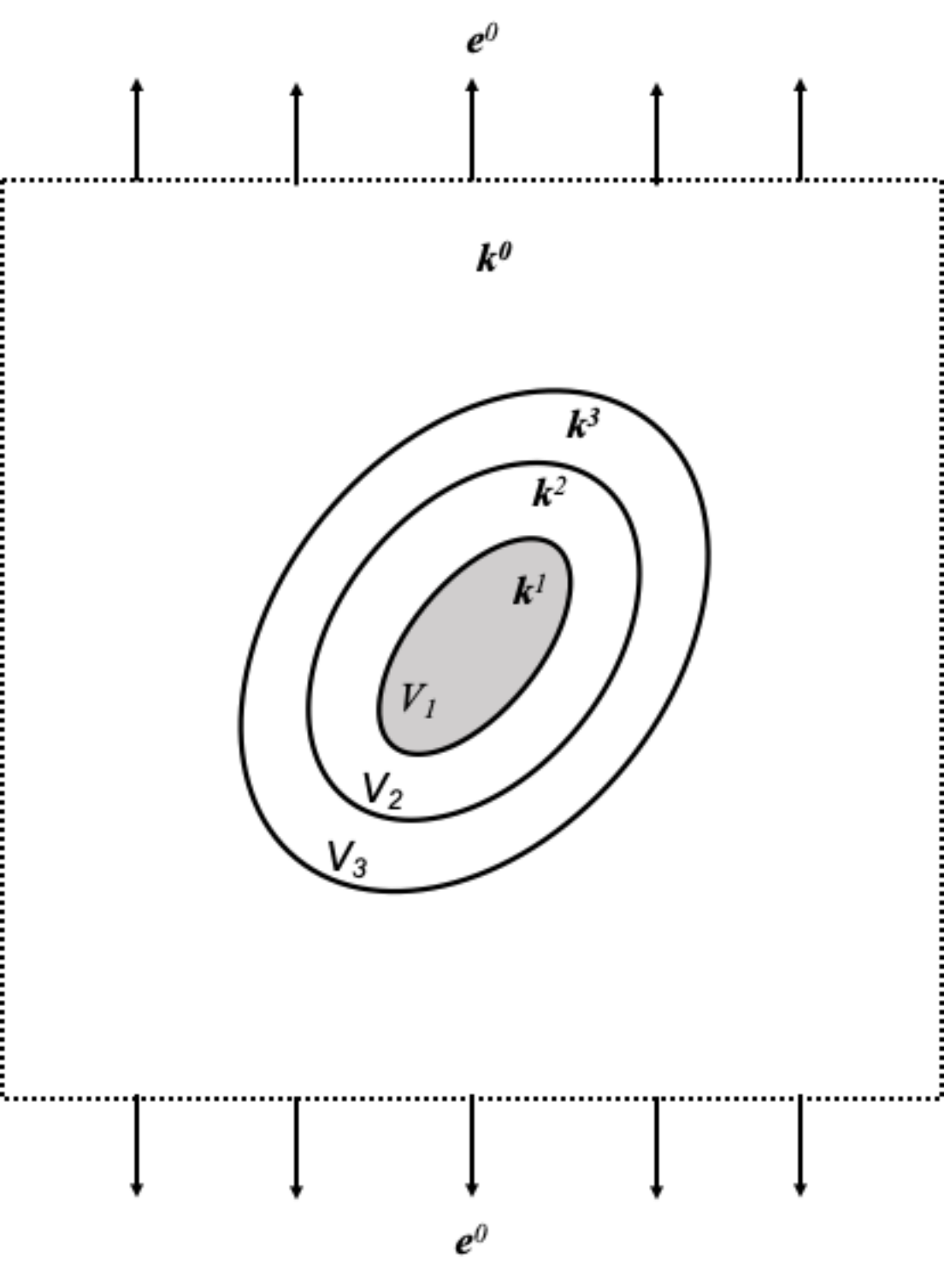
e^0
k^0
k^3
k^2
k^1
V_1
V_2
V_3
e^0

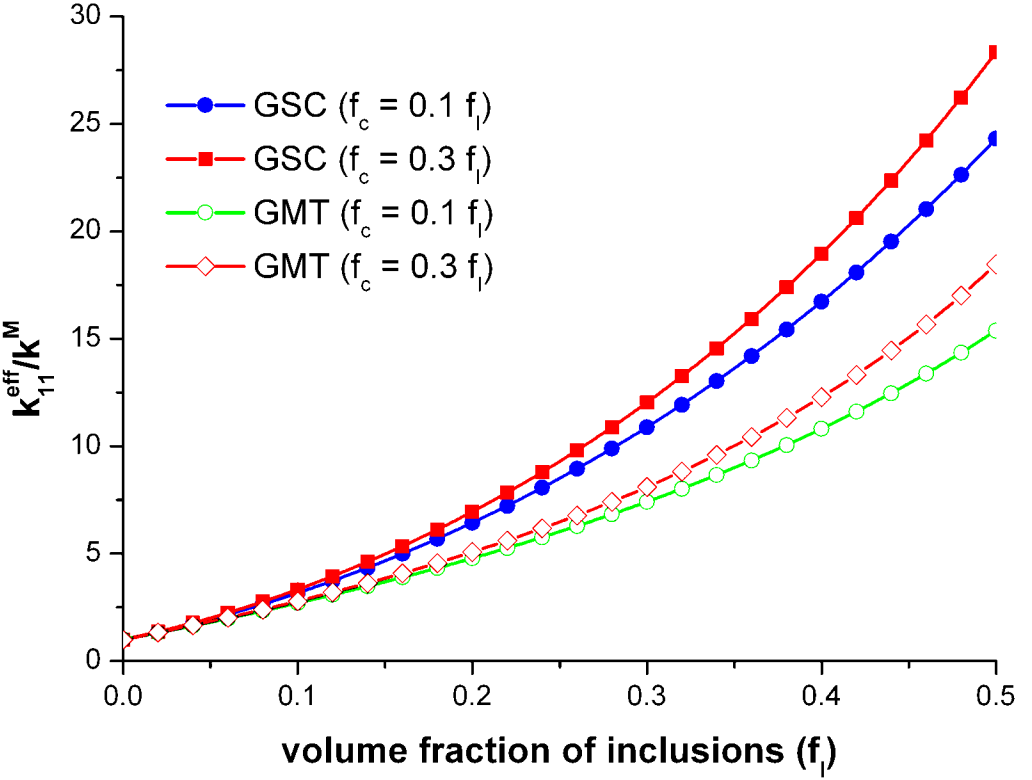
GSC (f_c = 0.1 f_I)
GSC (f_c = 0.3 f_I)
GMT (f_c = 0.1 f_I)
GMT (f_c = 0.3 f_I)
k_{11}^{eff}/k^M
volume fraction of inclusions (f_I)
0
5
10
15
20
25
30
0.0
0.1
0.2
0.3
0.4
0.5

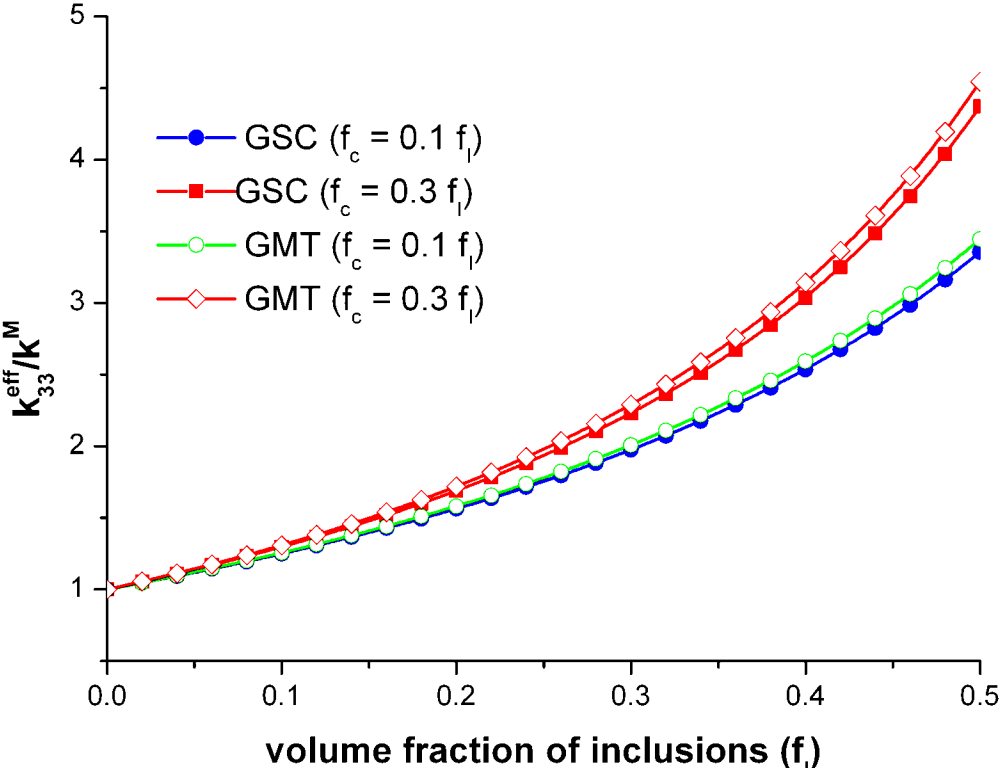
GSC (f_c = 0.1 f_I)
GSC (f_c = 0.3 f_I)
GMT (f_c = 0.1 f_I)
GMT (f_c = 0.3 f_I)
K_{33}^{eff}/K^M
volume fraction of inclusions (f_I)
0.0
0.1
0.2
0.3
0.4
0.5
1
2
3
4
5

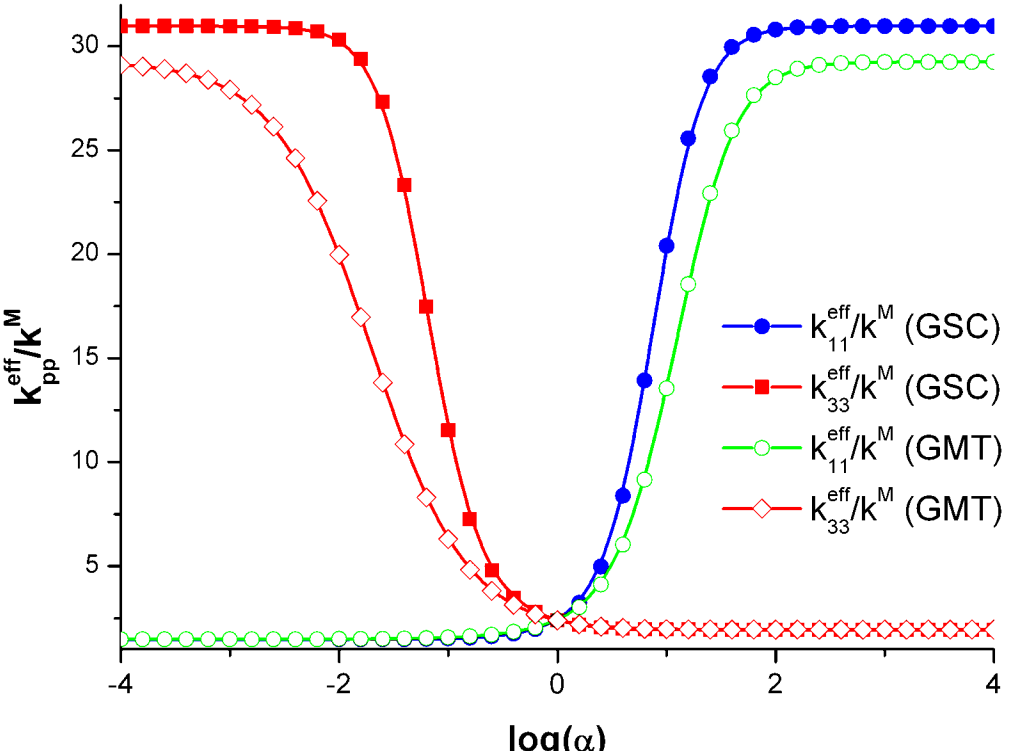
k_{pp}^{eff}/k^{M}
30
25
20
15
10
5
-4
-2
0
2
4
log(α)
k_{11}^{eff}/k^{M} (GSC)
k_{33}^{eff}/k^{M} (GSC)
k_{11}^{eff}/k^{M} (GMT)
k_{33}^{eff}/k^{M} (GMT)

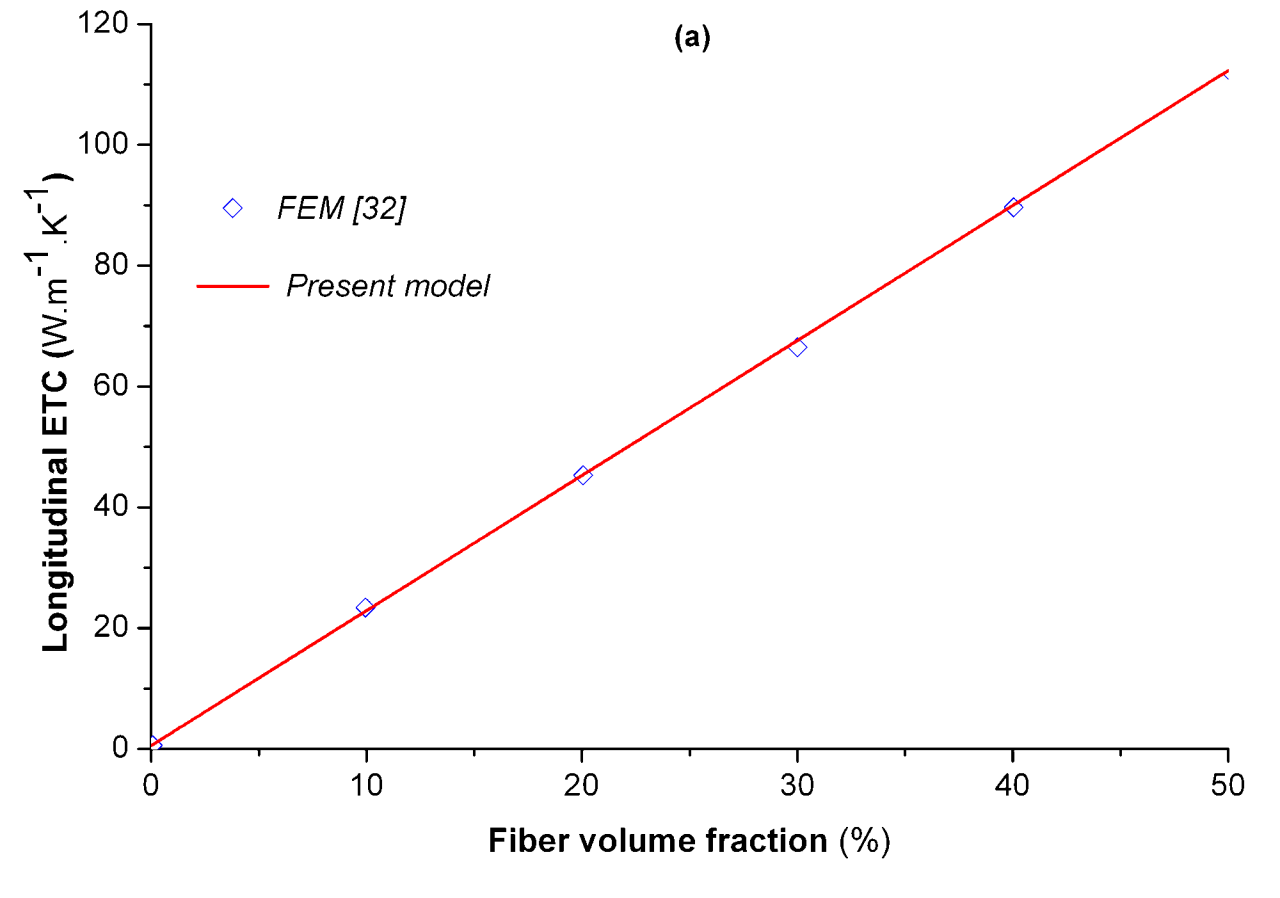
(a)
Longitudinal ETC (W.m-1.K-1)
FEM [32]
Present model
Fiber volume fraction (%)
0
20
40
60
80
100
120
0
10
20
30
40
50

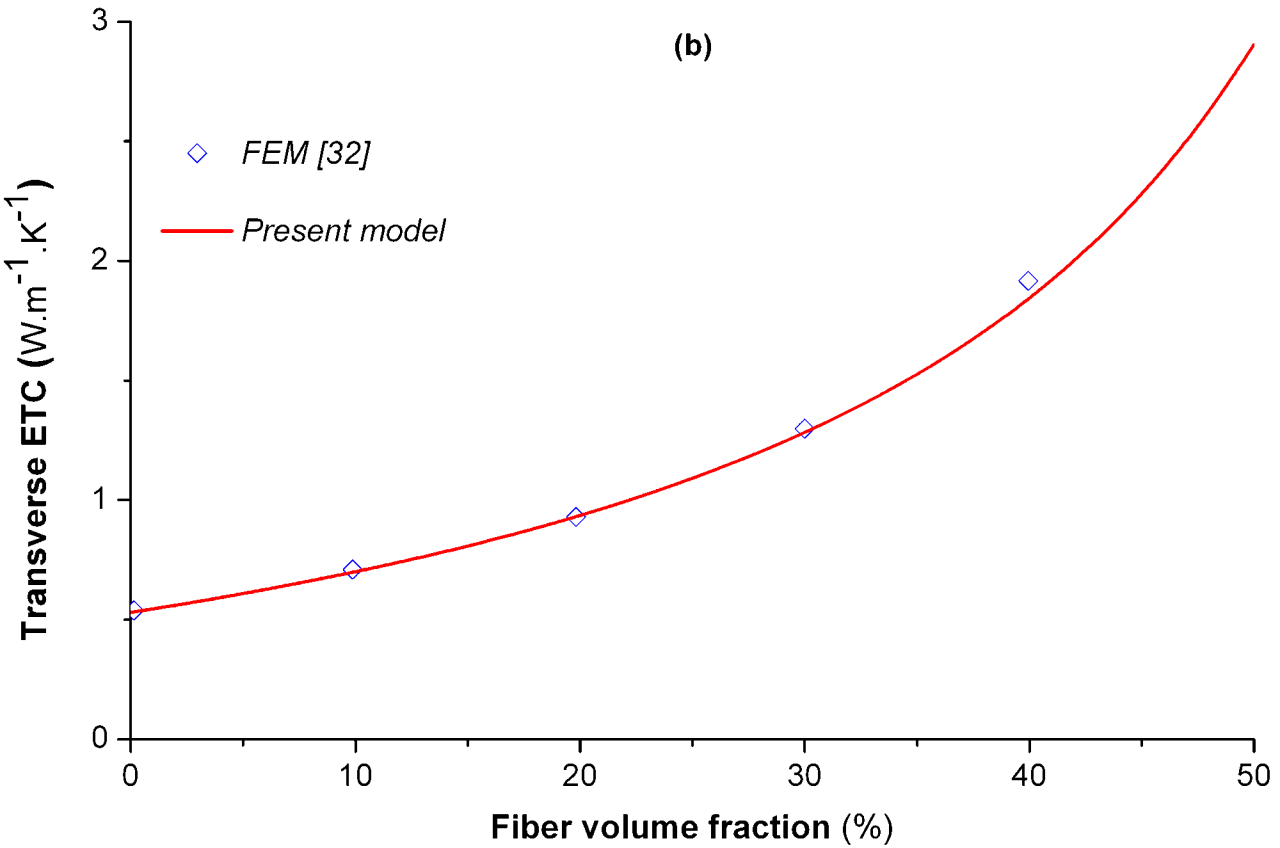
(b)
FEM [32]
Present model
Transverse ETC (W.m-1.K-1)
Fiber volume fraction (%)
0
1
2
3
0
10
20
30
40
50

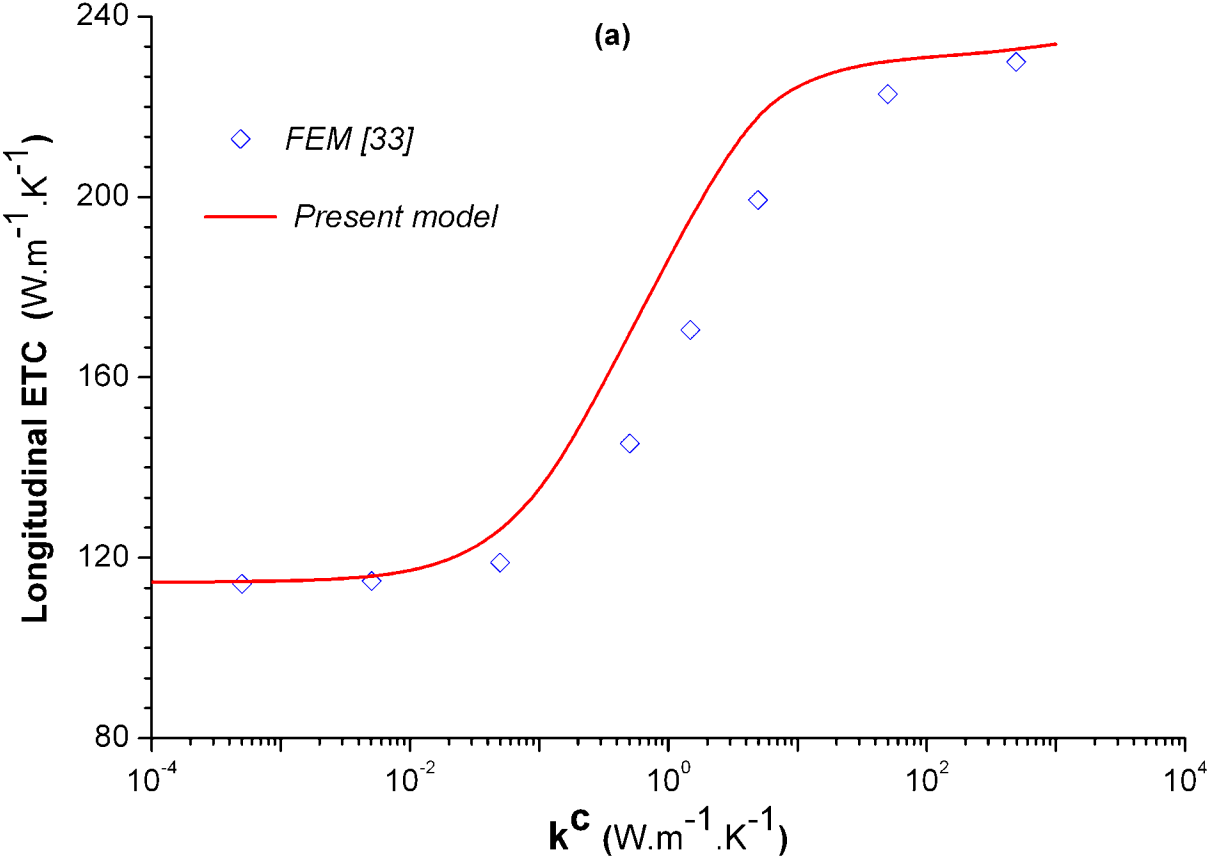
(a)
FEM [33]
Present model
Longitudinal ETC (W.m-1.K-1)
240
200
160
120
80
10-4
10-2
100
102
104
kc (W.m-1.K-1)

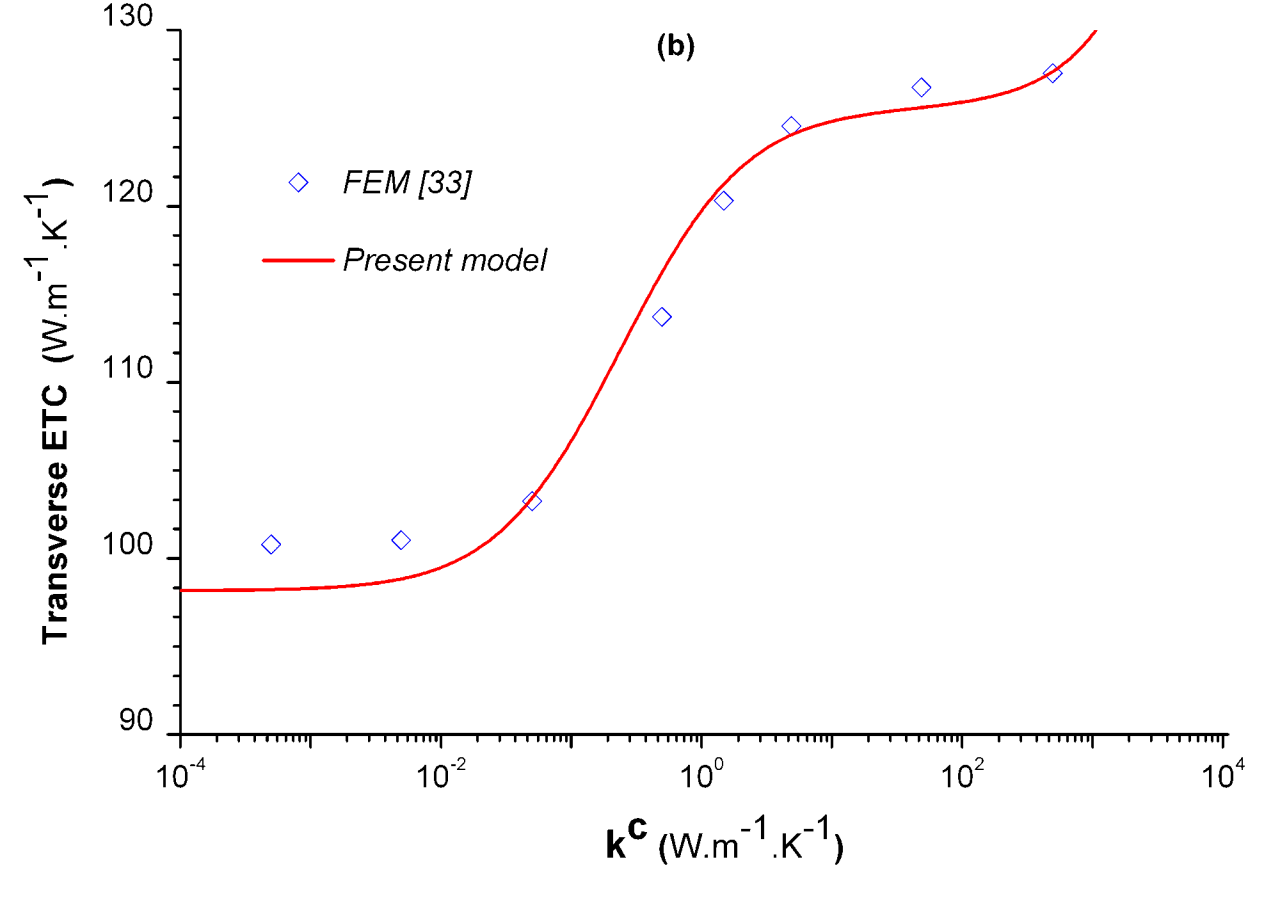
(b)
FEM [33]
Present model
Transverse ETC (W.m-1.K-1)
kc (W.m-1.K-1)
130
120
110
100
90
10-4
10-2
100
102
104

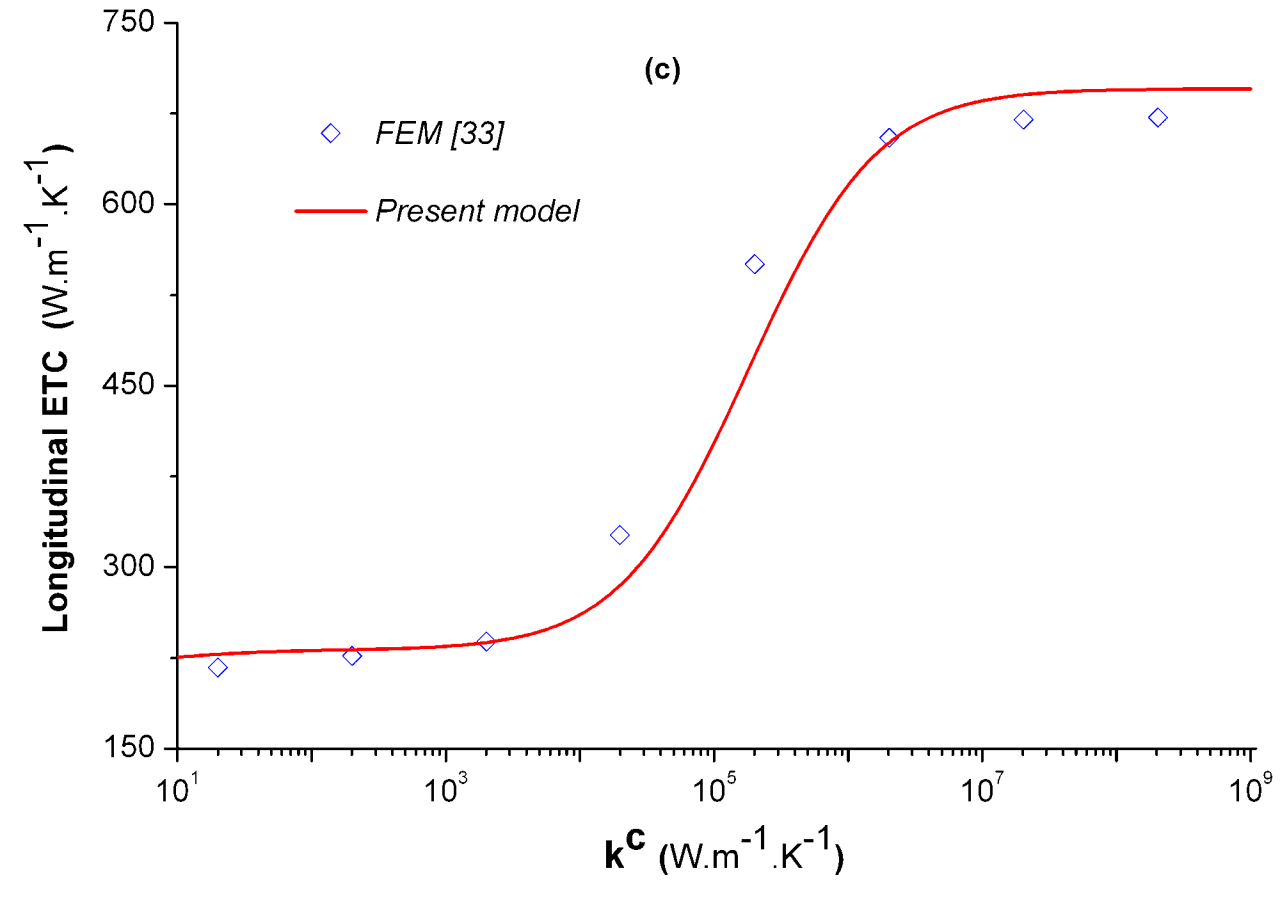
(c)
FEM [33]
Present model
Longitudinal ETC (W.m-1.K-1)
750
600
450
300
150
10^1
10^3
10^5
10^7
10^9
k^c (W.m-1.K-1)

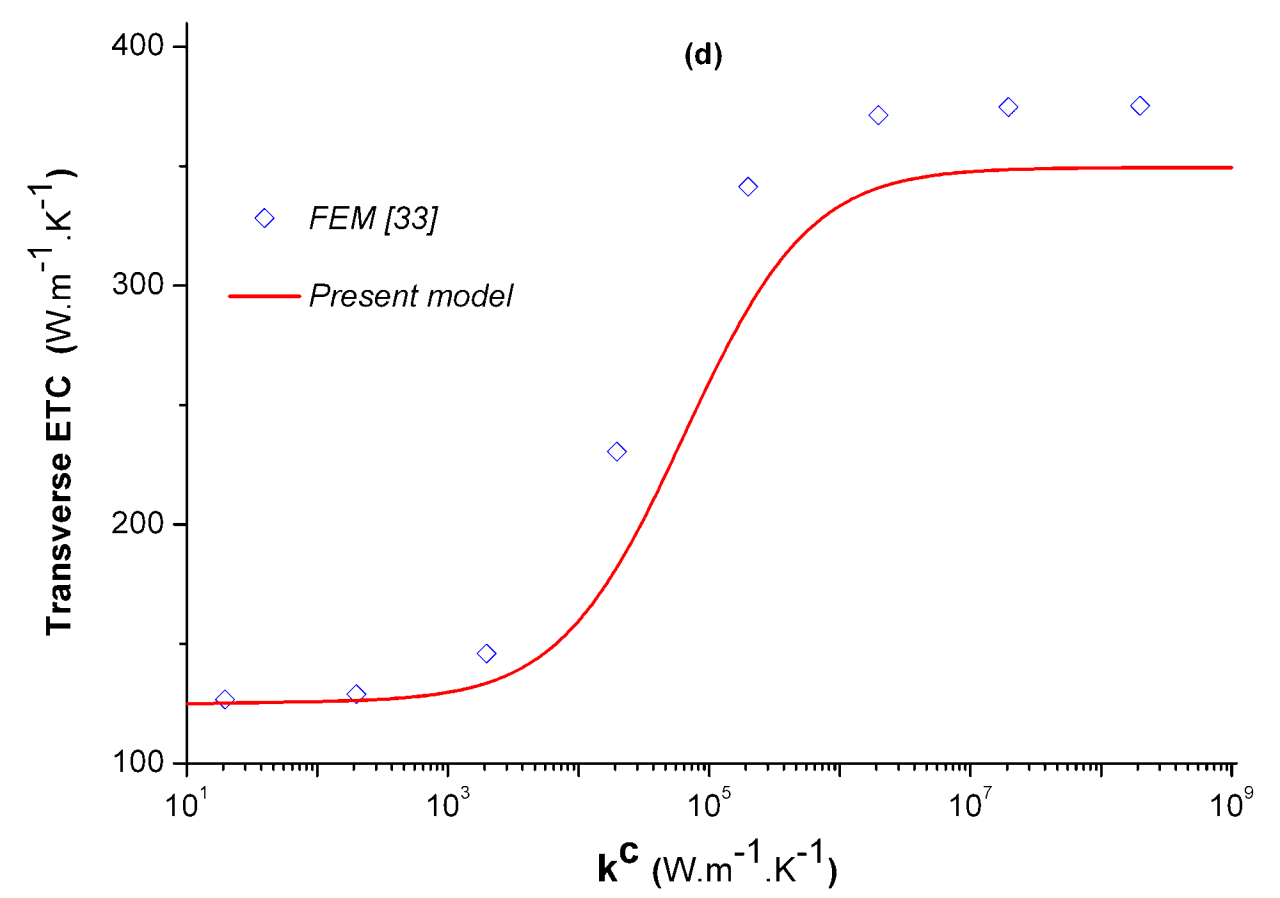
(d)
FEM [33]
Present model
Transverse ETC (W.m-1.K-1)
kc (W.m-1.K-1)
400
300
200
100
101
103
105
107
109

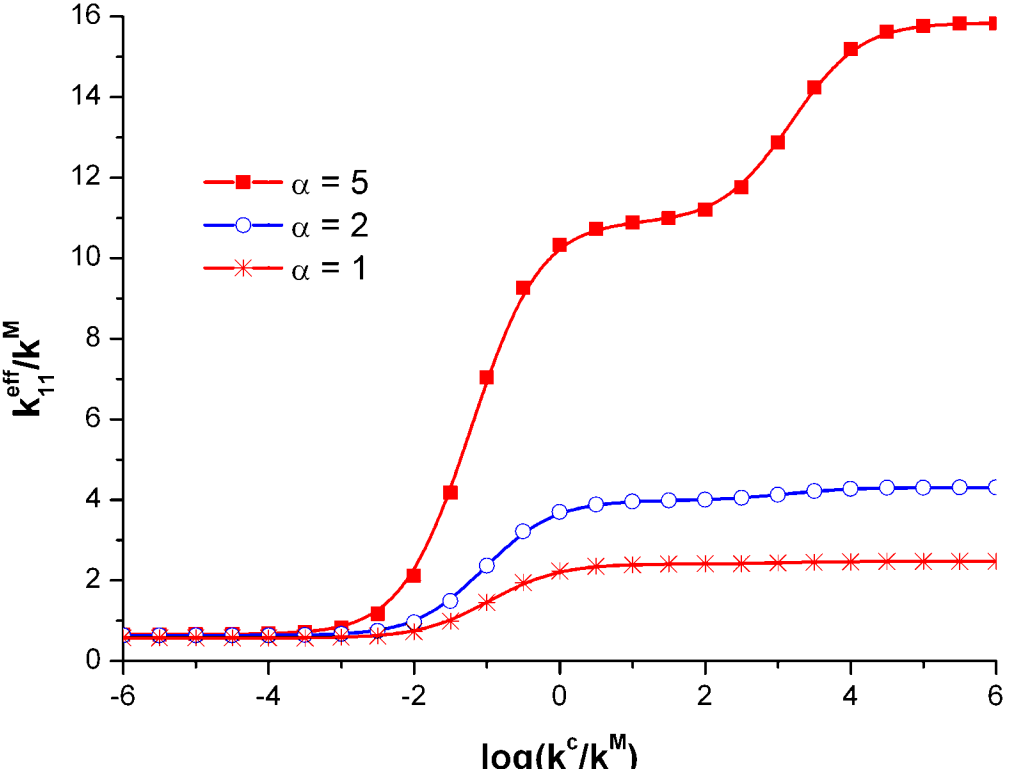
16
14
12
10
8
6
4
2
0
-6
-4
-2
0
2
4
6
α = 5
α = 2
α = 1
k_{11}^{eff}/k^M
$\log(k^c/k^M)$

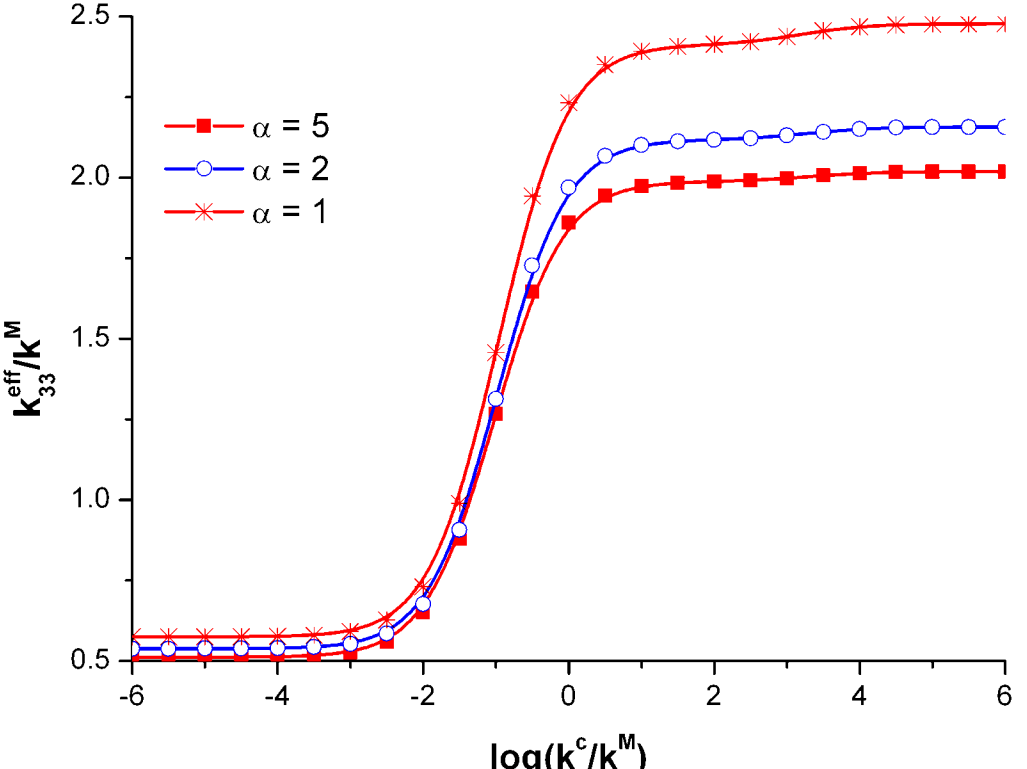
2.5
2.0
1.5
1.0
0.5
-6
-4
-2
0
2
4
6
α = 5
α = 2
α = 1
k_{33}^{eff}/k^M
$\log(k^c/k^M)$

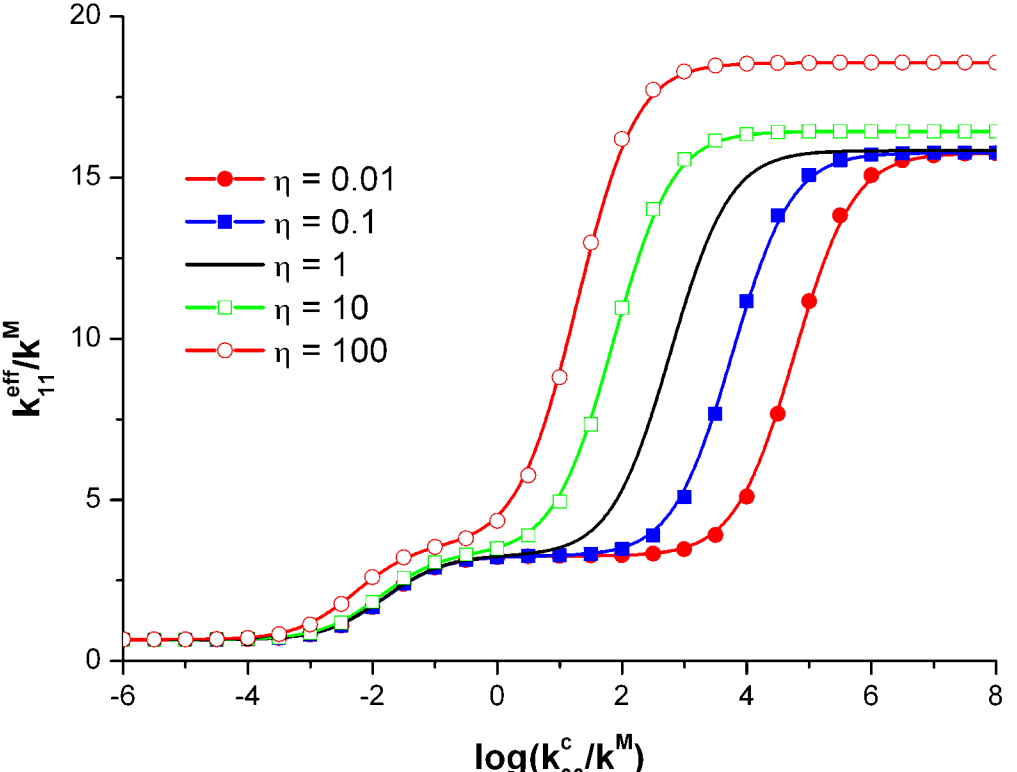
20
15
10
5
0
-6
-4
-2
0
2
4
6
8
η = 0.01
η = 0.1
η = 1
η = 10
η = 100
k_{11}^{eff}/k^{M}
$\log(k_{33}^{c}/k^{M})$

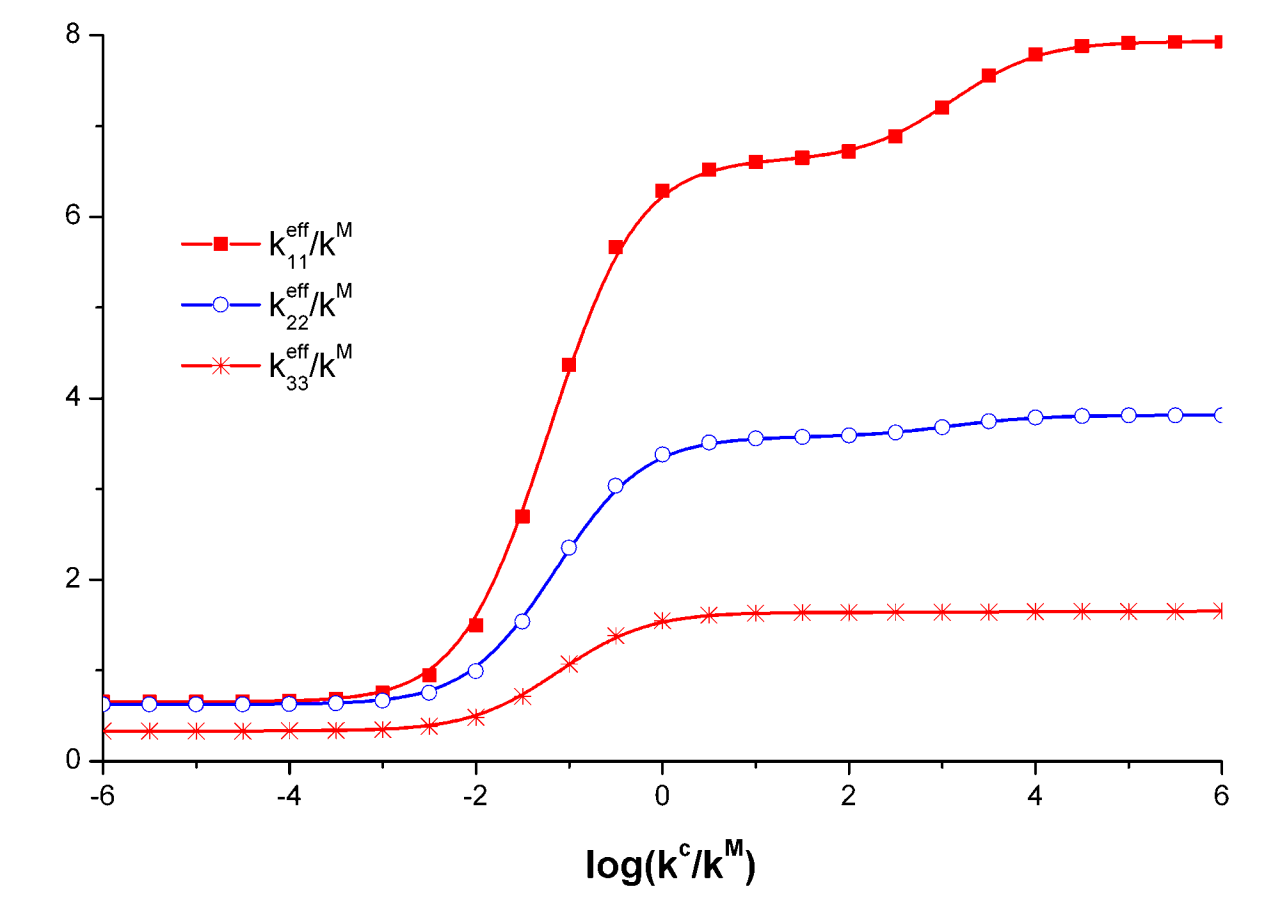
8
6
4
2
0
-6
-4
-2
0
2
4
6
k_{11}^{eff}/k^M
k_{22}^{eff}/k^M
k_{33}^{eff}/k^M
$\log(k^c/k^M)$